Cell

Syntaxin-4 Defines a Domain for Activity-Dependent Exocytosis in Dendritic Spines

Matthew J. Kennedy,[1] Ian G. Davison,[1,2] Camenzind G. Robinson,[1,2] and Michael D. Ehlers[1,2,*]
[1]Department of Neurobiology
[2]Howard Hughes Medical Institute
Duke University Medical Center, Durham, NC 27710, USA
*Correspondence: ehlers@neuro.duke.edu
DOI 10.1016/j.cell.2010.02.042

SUMMARY

Changes in postsynaptic membrane composition underlie many forms of learning-related synaptic plasticity in the brain. At excitatory glutamatergic synapses, fusion of intracellular vesicles at or near the postsynaptic plasma membrane is critical for dendritic spine morphology, retrograde synaptic signaling, and long-term synaptic plasticity. Whereas the molecular machinery for exocytosis in presynaptic terminals has been defined in detail, little is known about the location, kinetics, regulation, or molecules involved in postsynaptic exocytosis. Here, we show that an exocytic domain adjacent to the postsynaptic density (PSD) enables fusion of large, AMPA receptor-containing recycling compartments during elevated synaptic activity. Exocytosis occurs at microdomains enriched in the plasma membrane t-SNARE syntaxin 4 (Stx4), and disruption of Stx4 impairs both spine exocytosis and long-term potentiation (LTP) at hippocampal synapses. Thus, Stx4 defines an exocytic zone that directs membrane fusion for postsynaptic plasticity, revealing a novel specialization for local membrane traffic in dendritic spines.

INTRODUCTION

Rapid changes in membrane composition modify synapses during brain development and learning-related plasticity (Newpher and Ehlers, 2008; Shepherd and Huganir, 2007). At excitatory glutamatergic synapses in the mammalian brain, activity-dependent trafficking to and from the postsynaptic membrane controls synaptic strength and dendritic spine growth, and may mediate retrograde signaling (Kopec et al., 2007; Lledo et al., 1998; Luscher et al., 1999; Park et al., 2004, 2006; Tanaka et al., 2008; Yang et al., 2008b). Formative electrophysiological and imaging studies have found that exocytosis of internal membrane stores in dendrites is coupled to synaptic activity within minutes and is required for synaptic plasticity (Lledo et al., 1998; Maletic-Savatic and Malinow, 1998). However, the source of membrane, the site of membrane insertion, and the molecules involved are only beginning to emerge (Kennedy and Ehlers, 2006).

Principal among the molecules mediating membrane fusion are the soluble NSF-attachment protein receptor (SNARE) proteins, which attach intracellular vesicles to their target membranes and drive membrane fusion. Comprised of the syntaxin, SNAP-23/25, and synaptobrevin/VAMP protein families, SNARE proteins are essential for diverse forms of membrane fusion events in all eukaryotic cells (Jahn and Scheller, 2006; Martens and McMahon, 2008), and play a well known role in neurotransmitter release from presynaptic terminals (Sollner et al., 1993). Interestingly, *Clostridia* neurotoxins that cleave VAMP, SNAP-23/25, or syntaxin disrupt postsynaptic plasticity at excitatory synapses (Lledo et al., 1998; Lu et al., 2001), suggesting the presence of postsynaptic SNAREs. However, the SNARE molecules that mediate activity-dependent membrane trafficking in postsynaptic compartments remain unidentified.

In mammalian cells, four of the 15 members of the syntaxin family, Stx1-4, localize to the plasma membrane (PM), where they form small (50–60 nm) homotypic clusters of approximately 70 molecules that are thought to mark sites of exocytosis on the cell surface (Lang et al., 2001; Low et al., 2006; Ohara-Imaizumi et al., 2004; Sieber et al., 2006, 2007). Whereas Stx1 is localized to presynaptic terminals and mediates synaptic vesicle exocytosis, the roles of other syntaxins at synapses have not been defined.

In addition to a lack of information about relevant fusion machinery, the location of activity-driven postsynaptic exocytosis is controversial (Adesnik et al., 2005; Ashby et al., 2006; Kopec et al., 2007; Makino and Malinow, 2009; Park et al., 2006; Passafaro et al., 2001; Yudowski et al., 2007). Studies using an expressed GluR1 AMPA receptor subunit fused to the pH-sensitive GFP variant superecliptic pHluorin (SEP) revealed activity-dependent insertion of SEP-GluR1 at the soma and dendritic shaft, but failed to observe exocytosis directly within dendritic spines, the micron-sized membranous protrusions originating from the dendritic shaft that are the sites of excitatory synaptic contact (Makino and Malinow, 2009; Yudowski et al., 2007). Other studies demonstrated that both SEP-GluR1 and

transferrin receptor (TfR), a marker for recycling endosomal cargo, accumulate selectively on the spine PM following synaptic stimulation, suggesting that exocytosis takes place within or near spines (Kopec et al., 2006; Park et al., 2006). For membrane internalization in spines, dedicated zones of clathrin-mediated endocytosis positioned just lateral to the PSD have been identified (Blanpied et al., 2002; Lu et al., 2007; Racz et al., 2004). Thus, the presence of a spine exocytic zone would complete a micron-scale trafficking circuit that could set the composition of membrane proteins at individual synapses.

In the present study, we engineered an optical reporter for visualizing exocytosis and demonstrate that activity triggers abrupt, massive, all-or-none exocytosis of glutamate receptor-containing recycling endosomes (REs) in dendritic spines. High-resolution live cell imaging revealed that exocytosis occurs at discrete spine domains lateral to the postsynaptic density (PSD). These points of exocytosis coincide with submicron membrane clusters of Stx4, shown by immunogold electron microscopy to lie at membrane domains immediately lateral to the PSD. Further, both chronic and acute disruption of Stx4 inhibited activity-induced spine exocytosis and blocked long-term potentiation (LTP) at hippocampal synapses. Taken together, these results demonstrate activity-dependent exocytosis of recycling cargo, including glutamate receptors, at exocytic zones in spines, and they define Stx4 as a SNARE protein that directs membrane fusion for activity-dependent spine remodeling and synaptic plasticity. Establishment of a spine exocytic domain reveals a novel physiological function for Stx4 in coupling local signaling to spatially restricted membrane trafficking in cells.

RESULTS

An Optical Sensor for Exocytosis in Postsynaptic Compartments

To directly visualize postsynaptic exocytosis, we engineered a dual-color reporter by fusing transferrin receptor (TfR), a classic marker for recycling endosomal trafficking, to both mCherry (mCh) and the pH-sensitive GFP variant superecliptic pHluorin (SEP) (Miesenbock et al., 1998). This reporter, TfR-mCh-SEP, allowed us to image the entire pool of TfR in the red (mCh) channel and to selectively visualize only those TfR molecules at the PM in the green (SEP) channel, thus allowing visualization of exocytic cargo before, during, and following membrane fusion (Figure 1A and Figure S1 available online).

When TfR-mCh-SEP was expressed in hippocampal neurons (DIV17-20), we observed intracellular pools of TfR as large endosomal structures, typically 1–4 μm in length, in the dendritic shaft (Figures 1A and Figure S1). We also commonly observed smaller TfR-positive recycling endosomes (ranging in size from diffraction limited to ~0.5 μm in diameter) within 56% of dendritic spines (Figure 1B and Figure S1D). Spine endosomes labeled by TfR-mCh-SEP were stable under basal conditions and typically remained within the spine head for the length of our imaging sessions, which lasted up to 40 min. To confirm that the TfR-mCh-SEP spine compartments were functional, we imaged live cells expressing TfR-mCh-SEP after a 30 min saturating incubation with Alexa-647 conjugated transferrin (Alexa-Tf). Every TfR-mCh-SEP-positive endosome in spines became labeled with Alexa-Tf, indicating that intra-spine endosomes actively participate in ongoing recycling (Figure S1E). These data demonstrate that a large population of dendritic spines harbor one or more REs engaged in ongoing endocytic membrane trafficking.

AMPA Receptors Traffic through Spine-Localized Recycling Endosomes

To establish whether endogenous postsynaptic membrane proteins are trafficked through spine REs, we performed live-cell antibody feeding with an antibody directed against an N-terminal extracellular epitope of the GluR1 AMPA receptor. Live hippocampal neurons cotransfected with GFP and TfR-mCh (DIV 20-25) were incubated with anti-GluR1 for 3 hr at 37°C prior to fixation. Anti-GluR1 remaining at the cell surface was blocked with an unlabeled secondary antibody prior to permeabilization and labeling with Alexa647-conjugated secondary antibody to reveal internalized anti-GluR1 (Figure 1B). We observed that 85 ± 2% of spines containing TfR-mCh-labeled REs were also positive for internalized GluR1, while only 9 ± 4% of spines lacking TfR-mCh were positive for internalized GluR1 (Figures S1H and S1I). These TfR-negative compartments may represent GluR1-positive late endosomes (Ehlers, 2000).

We also tested whether exogenously expressed GluR1 was trafficked through spine REs by cotransfecting hippocampal neurons (DIV 20-25) with TfR-mCh and SEP-GluR1. Upon application of 50 mM NH_4Cl, we observed an increase in SEP-GluR1 signal that colocalized with spine REs in 42 ± 1% of endosome-containing spines, indicating that exogenously expressed SEP-GluR1 also traffics through spine REs, although much less efficiently than endogenous GluR1 (Figures S1G and S1H). Only 8 ± 4% of spines lacking TfR-mCh displayed an NH_4Cl-dependent increase in SEP-GluR1 (Figure S1I). Together, these findings demonstrate that internalized AMPA receptors are actively transported through spine REs.

Activity Triggers Exocytosis of Spine Endosomes Adjacent to the Postsynaptic Density

To assay whether endosomal compartments in spines are responsive to neuronal activity, we bathed neurons in Mg^{2+}-free solution containing 200 μM glycine, 30 μM bicuculline (Bic/Gly solution) for 5 min to increase total network activity. During and following incubation in Bic/Gly solution, intra-spine endosomes fused with the spine PM in large, dramatic exocytic events (Figure 1C and Movie S1). Exocytic events were characterized by a burst of SEP fluorescence indicating fusion, followed by a decline of SEP fluorescence with concomitant decay of mCh signal, interpreted as diffusion of newly inserted material away from the site of exocytosis (Figure 1C and Figure 2 and Movie S2). The frequency of spontaneous spine fusion events in the absence of Bic/Gly was low and increased several fold during and in the minutes following Bic/Gly exposure (Figure 1D). Nearly one third of dendritic spines containing a RE exhibited exocytosis following stimulation (30 ± 6%). To determine where exocytosis occurs in relation to the synapse, we performed high resolution imaging of neurons expressing TfR-SEP along with PSD-95-mCh to mark the location of the

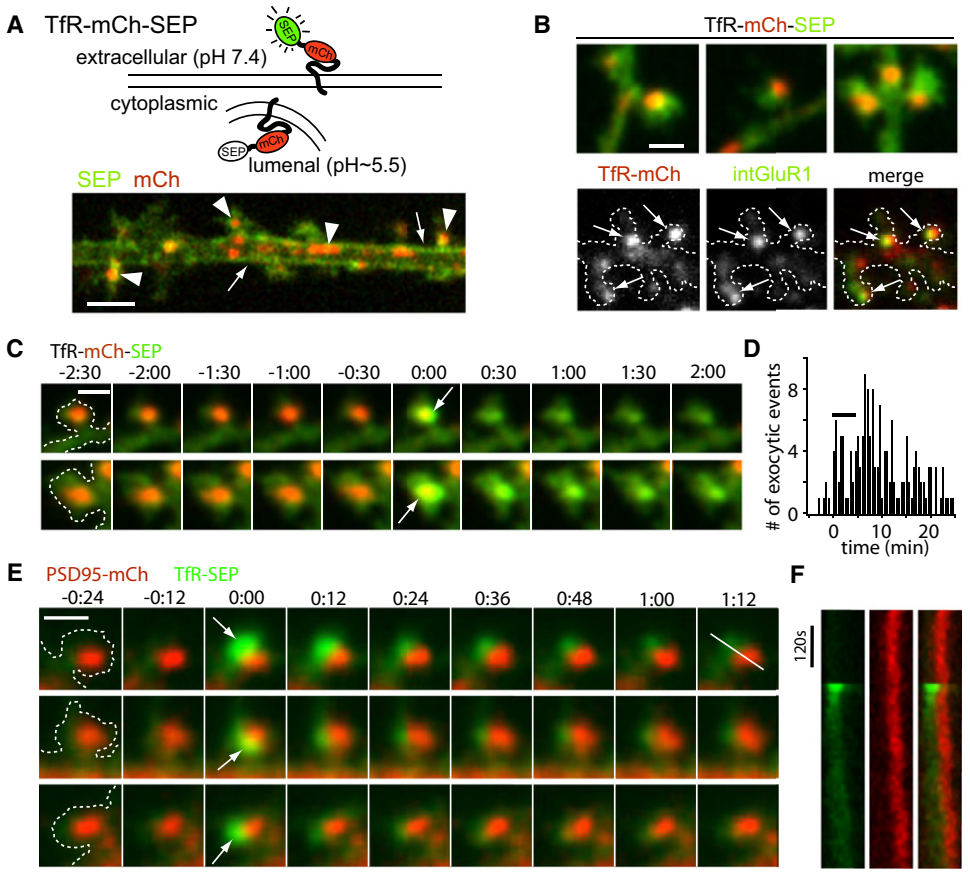

Figure 1. Activity Triggers Exocytic Fusion of Spine Endosomes at Sites Lateral to the PSD

(A) Schematic diagram of a dual color reporter for postsynaptic exocytosis. Transferrin receptor fused to mCherry (mCh) and superecliptic pHluorin (SEP) allows simultaneous visualization of total (mCh) and plasma membrane (SEP) TfR molecules. The lower panel shows a single confocal plane of a stretch of dendrite from a hippocampal neuron expressing TfR-mCh-SEP. Note the plasma membrane localization of the SEP signal (arrows) and the endosomal compartments in the red channel (arrowheads). The scale bar represents 4 μm.

(B) Spines harbor AMPA receptor-containing recycling endosomes (RE). Endosomes were observed in 56% of spines visualized with TfR-mCh-SEP (top panel). Live-cell antibody feeding with anti-GluR1 for 3 hr revealed internalized endogenous GluR1 (intGluR1) in 85 ± 2% of spine REs (bottom panels). The scale bar represents 1 μm.

(C) Intra-spine recycling endosomes visualized with TfR-mCh-SEP fuse with the spine PM (arrows) following stimulation with Bic/Gly. Two examples are shown. Two-color z stacks were acquired every 30 s and projected in 2 dimensions with the first frame of exocytosis assigned t = 0. Time is in min:sec. The scale bar represents 1 μm.

(D) Frequency of spine exocytosis increases with activity. Histogram analysis of spine exocytic events before, during, and following a 5 min treatment with Bic/Gly solution (horizontal bar). Data is binned in 30 s intervals. n = 160 spine exocytic events from 22 cells.

(E) Exocytosis occurs adjacent to the PSD. Cells expressing TfR-SEP (green) and the postsynaptic density marker PSD-95-mCh (red) were imaged following stimulation with Bic/Gly. Discrete spine exocytic events (white arrows) occurred adjacent to, but not directly overlapping, the PSD. Three representative events are shown. Time is in min:sec. The scale bar represents 1 μm.

(F) Kymograph analysis of TfR-SEP insertion adjacent to the PSD. Pixel intensity for the red (PSD95-mCh) and green channels (TfR-SEP) was measured along the line shown in (E) (last frame, top row). See also Figure S1 and Movie S1.

PSD. Nearly all spine fusion events (97%, n = 42) occurred within 300 nm of the edge of the PSD with little overlap between newly inserted TfR-SEP and PSD-95-mCh signal (Figures 1E and 1F and Movie S1). The average center-to-center distance between newly inserted TfR-SEP and PSD95-mCh was 361 ± 46 nm. Together, these findings demonstrate that stable REs in spines undergo abrupt, activity-dependent fusion that delivers exocytic cargo, including AMPA receptors, to the spine PM in close proximity to the PSD.

Recycling Endosomes Fuse with the Spine Plasma Membrane in an All-or-None Manner

Since exocytosis occurs at domains lateral to the PSD, we wondered how fast newly inserted molecules could become available to the synapse, and what fraction of endosomal cargo is inserted into the spine PM. To address these questions, we performed rapid time-lapse imaging of spine RE exocytosis in neurons expressing TfR-mCh-SEP following stimulation with Bic/Gly. In the first frame when fusion was detected by a burst

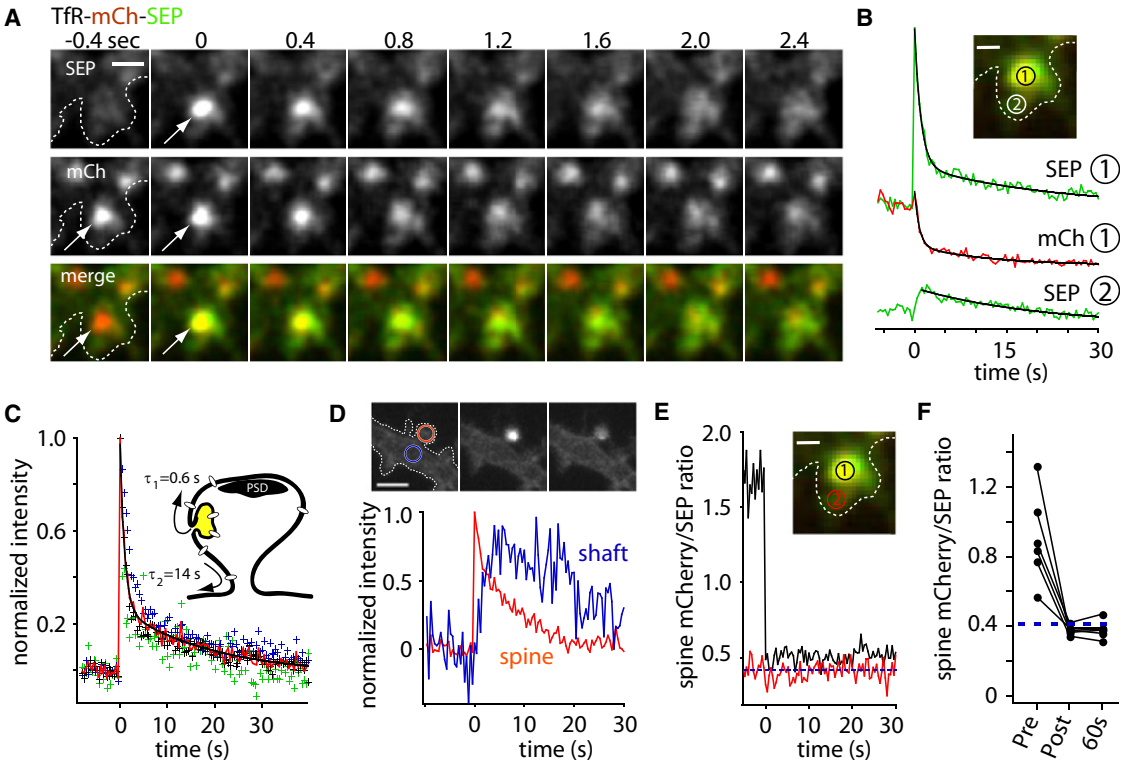

Figure 2. Spine Exocytosis Occurs In an All-or-None Manner

(A) Rapid two-color imaging of TfR-mCh-SEP showing stimulus-induced fusion of a recycling endosome at the spine PM (arrowheads). The scale bar represents 1 μm.

(B) Kinetics of TfR-mCh-SEP signal decay and diffusional loss following exocytosis in spines. The integrated fluorescence intensity was measured for mCh (red trace) and SEP (green trace) at the site of membrane fusion (inset, circle 1) and at a nonoverlapping region adjacent to the initial fusion site in the same spine (inset, circle 2; lower green trace). The scale bar represents 0.5 μm.

(C) The average SEP signal (red trace) for several exocytic events was fit with a double exponential function to yield the time constant for cargo release from the exocytic site (τ_1 = 0.6 ± 0.2 s) and subsequent exit from the spine head (τ_2 = 14 ± 2 s). A model for spine exocytosis is shown in the inset.

(D) Newly inserted cargo diffuses out of the spine head. TfR-SEP intensity was monitored in the spine head (red) and in the dendritic shaft (blue) immediately adjacent to the spine neck. The traces represent the average of 5 spine exocytic events.

(E) The ratio of mCh intensity to SEP intensity (mCh/SEP) was measured before and after spine exocytosis at region 1 (inset). The mCh/SEP ratio abruptly decreases upon exocytosis and remains near the empirically measured mCh/SEP_{neut} (dashed blue line). The red trace represents mCh/SEP at region 2 away from the fusion site (inset).

(F) The value of mCh/SEP before, immediately after, and 60 s after membrane fusion compared to mCh/SEP_{neut} (dashed blue line) for several exocytic events. See also Movie S2.

in SEP signal, the mCh signal remained unchanged compared to its pre-exocytosis value indicating that spine endosomes do not immediately collapse into the spine PM, but rather release cargo from the site of insertion over a period of several hundred milliseconds (Figures 2A–2C and Movie S2). As signal decayed from the original site of exocytosis, SEP and mCh intensity increased at adjacent sites within the spine head, suggesting that the initial, fast phase of fluorescence decay (τ_1 = 0.6 ± 0.2 s) represents cargo escape from the insertion domain (Figures 2B and 2C). At later time points, SEP and mCh fluorescence intensity decayed with identical kinetics (τ_2 = 14 ± 2 s) at both the fusion site and adjacent membrane domains, consistent with diffusion of TfR-mCh-SEP out of the spine head (Figure 2B). Following spine exocytosis we observed a delayed accumulation of SEP signal in the adjacent dendritic shaft (Figure 2D).

To determine the fraction of RE cargo that is released to the PM upon exocytosis, we took advantage of the intrinsic mCh/SEP fluorescence ratio of our reporter at neutral pH (mCh/SEP_{neut}) (Figure S1C). If a fraction of the reporter remains within endosomes, the mCh/SEP ratio will be greater than the ratio measured at neutral pH (mCh/SEP_{neut}), since the low pH environment of the endosome quenches SEP fluorescence with little effect on mCh fluorescence. Under our specific imaging conditions (laser intensities, EM-CCD gain and integration times) we determined mCh/SEP_{neut} to be 0.42 ± 0.02 (Figure S1C, see Experimental Procedures for details). To measure the fractional release of RE cargo, we thus monitored mCh/SEP ratio at the site of endosomal fusion. Prior to exocytosis, mCh/SEP was much greater than mCh/SEP_{neut}, but abruptly dropped to a value very near mCh/SEP_{neut} upon membrane fusion (Figure 2E), indicating that the entire complement of

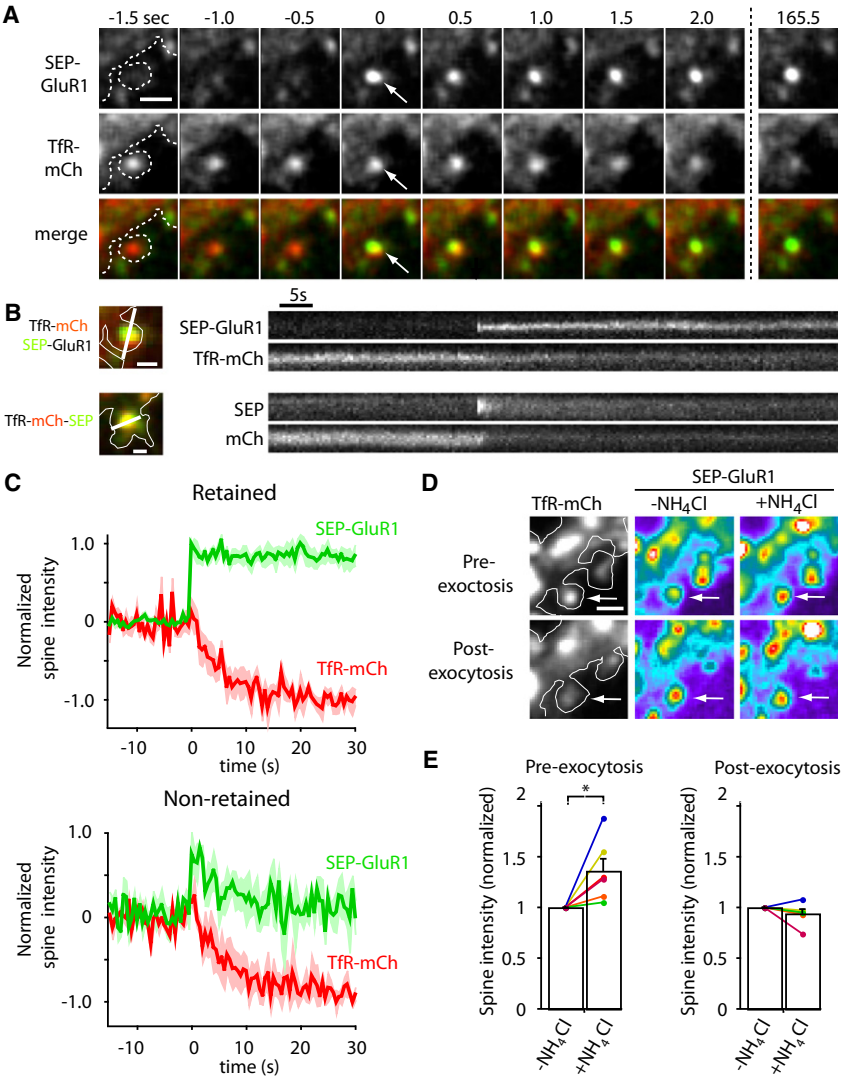

Figure 3. AMPA Receptors Are Directly Inserted into the Spine Plasma Membrane

(A) Time-lapse imaging of a hippocampal neuron coexpressing SEP-GluR1 (top row) and TfR-mCh (middle row) following stimulation with Bic/Gly. Note the abrupt appearance of SEP-GluR1 fluorescence at the precise location of a spine RE (arrows). The scale bar represents 1 μm.

(B) Kymograph comparison of newly inserted synaptic cargo. Shown are single exocytic events of SEP-GluR1 (top) and TfR-mCh-SEP (bottom). Note that SEP-GluR1 is inserted and retained in the spine head (upper kymograph), even as TfR-mCh from the same endosome quickly diffuses away with similar kinetics as newly exocytosed TfR-mCh-SEP (lower kymographs). The scale bar represents 0.5 μm.

(C) SEP-GluR1 exocytic events fall into two classes. Following RE fusion, SEP-GluR1 was either retained in spines (62% of events, top panel) or quickly diffused away (38% of events, bottom panel). In all cases, colocalized TfR-mCh signal (red traces) declined rapidly following the exocytosis of SEP-GluR1 (green traces).

(D) Exocytosis of SEP-GluR1 occurs in an all-or-none manner. Prior to stimulation, cells were treated with 50 mM NH_4Cl to reveal SEP-GluR1 within spine REs. Following RE exocytosis, NH_4Cl had no effect on SEP-GluR1 intensity in the same spines indicating plasma membrane localization. The scale bar represents 1 μm.

(E) Normalized spine SEP-GluR1 fluorescence intensity with and without NH_4Cl before and after SEP-GluR1 exocytosis in the same spines (*$p < 0.05$, paired students t test). See also Movie S3.

endosomal cargo was neutralized and became accessible to the extracellular media. If a portion of spine RE cargo were to remain in nonexocytosed compartments, this would be detected as mCh/SEP values greater than mCh/SEP_{neut}. However, we did not detect a measurable pool of intracellular TfR-mCh-SEP in spines following exocytosis (Figures 2E and 2F), arguing against the presence of additional nonexocytosing endosomal compartments in spines and indicating that new spine REs are not rapidly reformed following exocytosis.

AMPA Receptors Are Stably Inserted into the Spine Plasma Membrane via Fusion of Spine Endosomes

To determine whether exocytosis of spine REs delivers synaptic molecules to the spine PM, we imaged live hippocampal neurons expressing both TfR-mCh and SEP-GluR1. Following stimulation with Bic/Gly, we often observed the abrupt appearance of SEP-GluR1 signal in TfR-mCh-positive spines immediately followed by decay of TfR-mCh signal (Figures 3A–3C). Following a rapid burst of SEP-GluR1 fluorescence, newly inserted receptors either quickly diffused out of the spine (38% of the events) or remained in the spine head at nearly the same intensity for the remainder of the imaging session (62% of the events) (Figure 3C and Movie S3). In all cases, co-localized TfR-mCh signal diffused out of the spine immediately following the appearance of SEP-GluR1, even if newly inserted SEP-GluR1 was retained near the site of fusion (Figures 3A–3C and Movie S3). Because fusion of spine REs occurs in an all-or-none manner, we tested whether endosomal GluR1 was fully depleted following exocytosis in individual spines. Cells were treated with 50 mM NH_4Cl before stimulation and following exocytosis to determine the content of SEP-GluR1 in spine REs. Prior to stimulation, NH_4Cl treatment increased RE-localized SEP-GluR1 intensity. Following exocytosis, NH_4Cl treatment had no effect on SEP-GluR1 intensity in the same spines, indicating that exocytosis of spine REs depletes the entire supply of endosomal GluR1 (Figures 3D and 3E). Together, these findings demonstrate that AMPA receptors present in spine REs are directly exocytosed in an all-or-none manner at the spine plasma membrane where they can be stably incorporated.

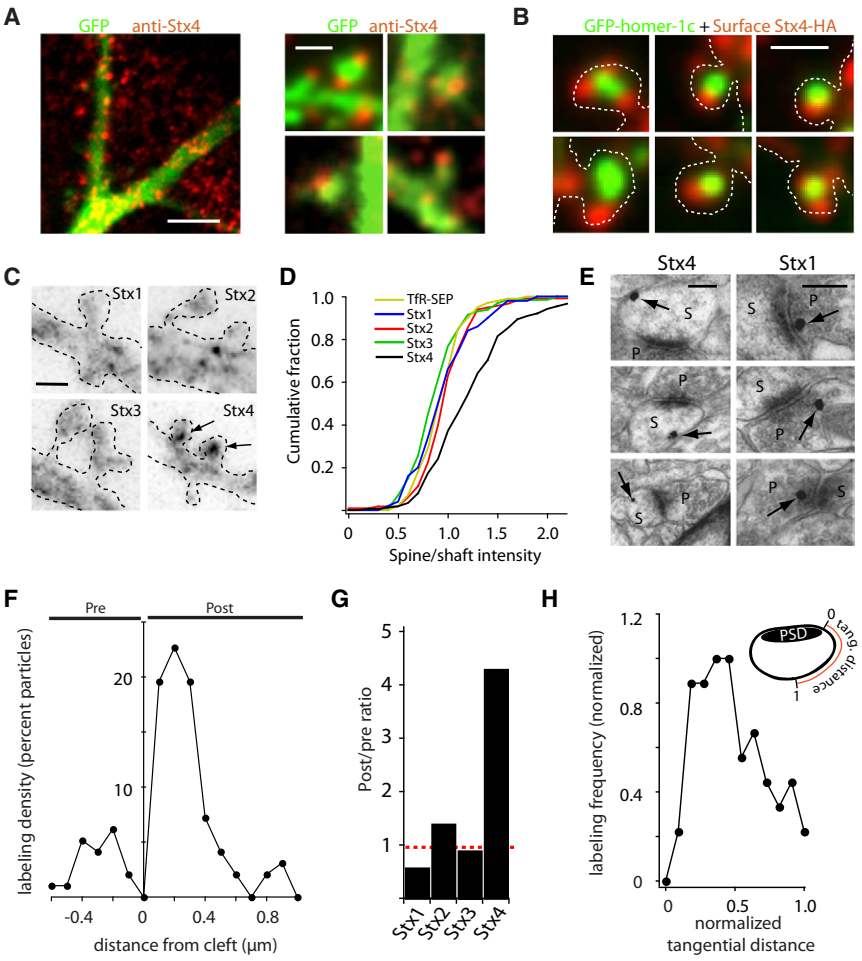

Figure 4. Syntaxin 4 Localizes to Lateral Spine Domains

(A) Subcellular localization of Stx4 in neurons. Hippocampal neurons (DIV18) expressing GFP as a cell fill (green) were stained with an antibody against Stx4 (red). Right panels show several examples of Stx4 label in dendritic spines. The scale bars represent 5 μm, left panel; 1 μm, right panels.

(B) Surface labeling of Stx4-HA. Hippocampal neurons expressing GFP-homer1c (green) and Stx4-HA (red) were fixed and incubated with anti-HA under nonpermeabilizing conditions to label surface Stx4. The scale bar represents 1 μm.

(C) Stx4 is enriched in spines. Neurons expressing HA-tagged Stx1-4 were surface labeled with anti-HA antibody. Arrows indicate spine-enriched Stx4-HA. Dashed lines indicate the cell outline. The scale bar represents 1 μm.

(D) Cumulative distribution of spine/shaft ratios for surface labeled syntaxins 1-4. TfR-SEP served as a control for an evenly distributed membrane protein. (n = 160, 122, 130, 210 spine/dendrite pairs from at least 5 different cells for Stx1-4, respectively).

(E) Pre-embedding immunogold labeling of adult rat hippocampus with anti-Stx4 and anti-Stx1. Representative examples of Stx4 (left) and Stx1 (right) labeling (arrows) are shown. Abbreviations: p, presynaptic terminal; s, spine. The scale bars represent 200 nm.

(F) Quantitative analysis of Stx4 distribution at asymmetric synapses. The distance of individual gold particles from the synaptic cleft was measured with negative and positive values representing particles at presynaptic and postsynaptic sites, respectively. n = 115 particles.

(G) Postsynaptic-to-presynaptic ratios of endogenous plasma membrane syntaxins at asymmetric synapses determined by immunogold labeling. The total number of postsynaptic gold particles was divided by the total number of presynaptic gold particles. (n = 97, 70, 95, 115 synaptic particles for syntaxins 1–4 respectively).

(H) Stx4 concentrates at lateral spine domains. Shown is the normalized tangential distance of postsynaptic Stx4 labeling along the plasma membrane from the edge of the PSD (0) to the most distant point from the PSD along the spine plasma membrane (1). See also Figure S2.

Syntaxin 4 Is a Postsynaptic t-SNARE at Glutamatergic Synapses

To identify the molecular basis for postsynaptic membrane fusion, we searched for SNARE proteins expressed in brain that localize near the postsynaptic PM. Of the four PM syntaxins, Stx1 and Stx4 are expressed at high levels in the brain (Allen Brain Atlas, http://www.brain-map.org). Stx1 localizes presynaptically where it mediates synaptic vesicle exocytosis. The function(s) of Stx4 in brain is unknown. Immunolabeling of rat brain sections with antibodies against Stx4 revealed widespread Stx4 protein expression throughout the brain including hippocampus and neocortex (Figure S2A). Biochemical fractionation revealed both Stx1 and Stx4 in synaptosome fractions from adult mouse brain (Figure S2B). Consistent with previous studies (Takamori et al., 2006), Stx1 was abundant in synaptic vesicle fractions, while Stx4 was largely absent from this fraction (Figure S2B). Thus, Stx4 is present in synaptic fractions but not synaptic vesicles.

To examine the subcellular distribution of Stx4 in neurons, we performed immunocytochemical labeling of hippocampal neurons, which revealed a punctate distribution of Stx4 throughout the somatodendritic compartment (Figure 4A) in agreement with previous studies in nonneuronal cells (Low et al., 2006; Sieber et al., 2007). Stx4 clusters often localized to dendritic spines (Figure 4A), and most dendritic spines contained at least one punctate spot of Stx4 in the spine head or spine neck. To allow selective visualization of Stx4 at the plasma membrane, we expressed Stx4 fused to an extracellular HA tag. Surface labeling revealed that Stx4-HA puncta were in close proximity, but seldom overlapped with the PSD marker homer1c (Figure 4B). Centroid analysis revealed an average separation of 356 ± 41 nm between spine Stx4 clusters and the center of the PSD, a value nearly identical to the distance between newly inserted TfR-SEP and the center of the PSD (361 ± 46 nm). Out of all PM syntaxins, only Stx4-HA was enriched in spines with clusters at the PM of nearly every dendritic spine (95 ± 4%) (Figures 4C and 4D).

To determine whether endogenous Stx4 resides postsynaptically in vivo, we performed immunogold electron microscopy

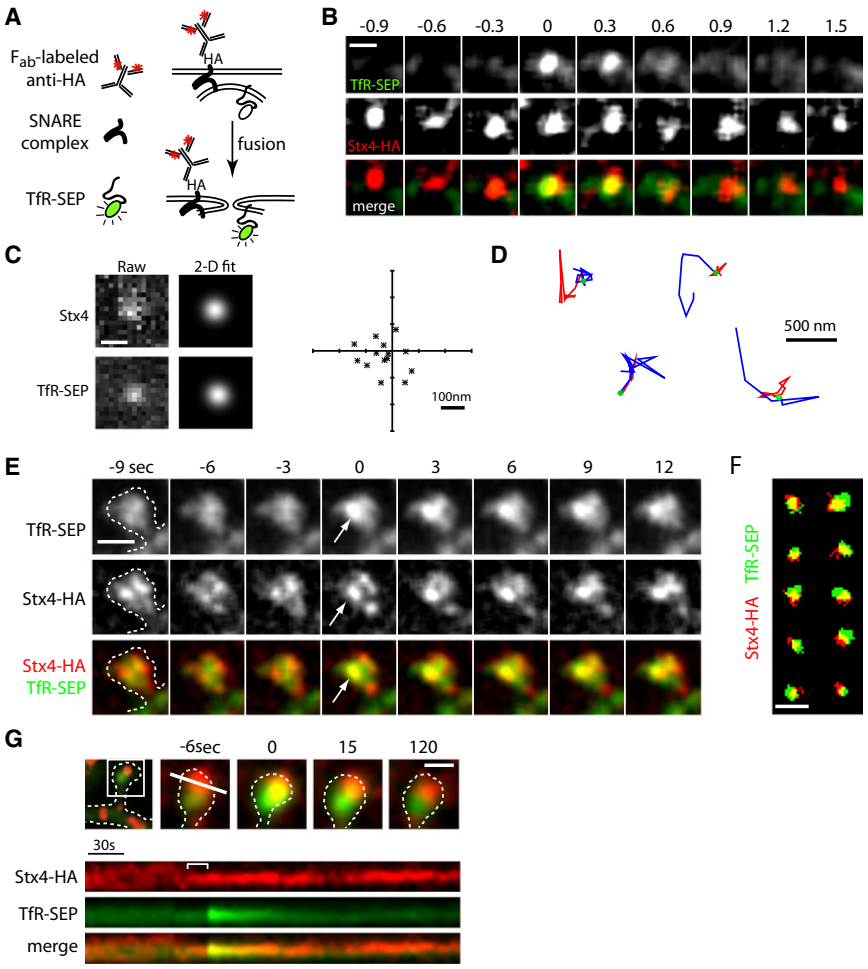

Figure 5. Stx4 Marks Sites of Exocytosis at the Spine Membrane

(A) Schematic diagram illustrating the method of labeling surface Stx-HA using anti-HA antibody and Cy3-conjugated monovalent anti-mouse F_{ab} fragments together with visualization of exocytic events using TfR-SEP.

(B) Exocytosis of RE cargo occurs at Stx4 clusters. TfR-SEP (top row) and surface Stx4-HA (middle row) signals were imaged during spontaneous TfR-SEP exocytic events in COS7 cells. The scale bar represents 500 nm.

(C) Stx4 clusters and TfR-SEP signal were fit with a 2-dimensional Gaussian function to determine their relative centroid positions. Raw data (left) and 2-D Gaussian fits (right) are shown. Scale bar, 500 nm. The graph plots the centroid separation for each paired TfR-SEP/Stx4 event (asterisks) with the Stx4 cluster held as the origin for 14 different exocytic events. The mean centroid separation was 83 ± 11 nm.

(D) Labeled Stx4 clusters are mobile. Trajectories of four different surface labeled Stx4 clusters preceding (red), during (filled green circle) and following (blue) TfR-SEP exocytosis over 7.6, 7.6, 5.6, and 14.4 s intervals (from left to right).

(E) Newly inserted TfR-SEP colocalizes with Stx4 clusters in spines. Hippocampal neurons expressing TfR-SEP (top row) and Stx4-HA were labeled with anti-HA antibody and Cy3-conjugated anti-mouse F_{ab} fragments to mark surface clusters of Stx4 (middle row) as in (B). Discrete exocytic events occur at pre-existing clusters of surface Stx4 (arrows). The scale bar represents 1 μm.

(F) Spatial distribution of surface Stx4 and newly inserted TfR-SEP in dendritic spines. Signals for TfR-SEP (green) and Stx4 (red) were binarized by thresholding the images at 20%–30% above background for 10 different spine exocytic events. The scale bar represents 1 μm.

(G) Kymograph analysis of TfR-SEP insertion (green) at the labeled Stx4 cluster (red) shown in the top panels. Note the coalescence of the Stx4 cluster (bracket, top kymograph) preceding exocytosis. See also Figure S3 and Movie S4.

(EM) focusing on stratum radiatum of area CA1 of rat hippocampus, using antibodies against all plasma membrane syntaxins (1–4). Stx4 label was often found near the spine membrane at sites lateral to the PSD (Figures 4E and 4F). Occasional labeling was observed presynaptically, but quantitative analysis revealed a 4-fold postsynaptic enrichment of Stx4 (Figures 4F and 4G). In contrast, Stx1 immunogold labeling was enriched 2-fold in presynaptic compartments, while Stx2 and Stx3 were evenly distributed between the pre and postsynaptic compartments (Figure 4G and Figure S2C). Analysis of the tangential distribution of postsynaptic Stx4 signal along the spine PM revealed a strong peak of labeling in lateral domains (Figure 4H) consistent with Stx4 enrichment just outside of the PSD.

Spine Exocytosis Occurs at Syntaxin-4 Clusters

To assess whether exocytosis of recycling cargo occurs at Stx4 clusters, we labeled surface Stx4-HA and monitored insertion of TfR-SEP in COS7 cells. Surface Stx4-HA was visualized by sequential incubation with anti-HA and a monovalent goat anti-mouse F_{ab} conjugated to Cy3 (Figure 5A). Surface-labeled Stx4 appeared as small mobile clusters (Figure S3 and Movie S5) that recovered rapidly when a small region of the cell was photobleached (Figure S4E). When we used Cy3-conjugated whole IgG to label surface Stx4 in live cells, we observed large, immobile aggregates that failed to recover when a small region of the cell was photobleached (Figures S4D and S4E and Movie S5) due to crosslinking induced by the bivalent IgG.

To test if exocytosis occurs directly at Stx4 clusters, we coexpressed Stx4-HA with TfR-SEP in COS7 cells and visualized surface Stx4 while monitoring spontaneous delivery of TfR-SEP to the PM (Figures 5B–5D). For the majority of exocytic events observed (16/26), newly appearing TfR-SEP signal tightly colocalized with Stx4 clusters (Figures 5B and 5C and Movie S4). These events were rapid, small, and occurred either directly at or within diffraction-limited proximity to Stx4-HA. High-resolution analysis revealed an average centroid separation of newly

appearing TfR-SEP spots and Stx4-HA clusters of 83 ± 11 nm (Figure 5C). Interestingly, Stx4-HA clusters exhibited small lateral displacements in the membrane that slowed or ceased immediately prior to an exocytic event (Figure S3 and Movie S4), consistent with a physical association with v-SNAREs on the incoming endosome immediately prior to fusion. Furthermore, Stx4 cluster intensity increased in the seconds preceding exocytosis, likely indicating local recruitment of Stx4 molecules and engagement of the SNARE complex (Figure S3).

Given that Stx4 is present in spines near glutamatergic synapses (Figure 4), we asked whether spine exocytic events occur at dedicated domains containing Stx4. To this end, we performed two-color time-lapse imaging of hippocampal neurons expressing Stx4-HA and TfR-SEP, visualizing surface Stx4 labeled using anti-HA antibody and exocytic events by SEP fluorescence. During live imaging, we observed the sudden appearance of bright TfR-SEP puncta that overlapped with labeled Stx4 in individual spines (Figures 5E–5G and Movie S4). These events were intermittent, rapid, and occurred within diffraction-limited proximity to Stx4-HA (Figures 5F and 5G). High-resolution analysis revealed an average centroid separation of newly appearing TfR-SEP spots and Stx4-HA clusters of 158 ± 31 nm at the time of membrane fusion. Following the sudden appearance of TfR-SEP spots, the bright fluorescence dispersed away from Stx4-HA clusters, diffusing out of the spine (Figure 5G and Movie S4). In many cases we observed coalescence of the Stx4 signal a few seconds before exocytosis (Figure 5G and Figures S3B and S3C). Together, these results demonstrate that recycling endosome fusion occurs at concentrated zones of Stx4 in dendritic spines, indicating that Stx4 defines a SNARE-based exocytic domain for rapid modification of the spine membrane.

Syntaxin 4 Mediates Activity-Triggered Exocytosis in Dendrites and Spines

To test whether Stx4 is required for activity-triggered postsynaptic exocytosis, we first knocked down endogenous Stx4 using shRNA (Figures S4A–S4C) and measured activity triggered exocytosis. Hippocampal neurons were transfected with Stx4 shRNA or a scrambled shRNA control along with TfR-SEP as a reporter for exocytosis for 72–96 hr, a time when Stx4 has been reduced to 25%–30% of its original level (Figure S4). For neurons expressing scrambled shRNA, stimulation with Bic/Gly trigged a robust increase in surface TfR-SEP signal on dendrites and spines that was blocked by the NMDA receptor antagonist APV (Figures 6A and 6B). The activity-induced increase in surface TfR-SEP was nearly completely blocked in cells expressing either one of two shRNA constructs directed against Stx4 (Figure 6A).

As an alternative strategy, we used a dominant negative approach to disrupt Stx4 function by expressing a soluble fragment of Stx4 consisting of its cytoplasmic domain (amino acids 1–273) but lacking the transmembrane domain (Stx4ΔTM). Soluble Stx4ΔTM forms cognate SNARE complexes but is not associated with the membrane, and thus disrupts Stx4-dependent trafficking (Olson et al., 1997). We expressed either mCh alone or mCh fused to Stx4ΔTM along with TfR-SEP as a reporter for exocytosis in dendrites and spines for 24–48 hr. When mCh-Stx4ΔTM was coexpressed with TfR-SEP, we observed a much slower, smaller, and delayed accumulation of TfR-SEP on the PM, reaching a maximum steady state level of approximately 20% over initial surface TfR-SEP prior to stimulation (Figure 6B). Quantitative analysis revealed an 85 ± 6% inhibition of TfR-SEP surface accumulation at 3 min following stimulation and 62 ± 7% at 15 min following stimulation. The effect of Stx4ΔTM was specific, as expression of a soluble fragment of the related PM syntaxins, Stx1 and Stx3 (Stx1ΔTM and Stx3ΔTM), had no effect on activity-induced TfR-SEP insertion (Figure 6C).

Because knocking down Stx4 with shRNA or overexpressing mCh-Stx4ΔTM for extended times could have unanticipated secondary effects, we developed a method to selectively and rapidly disrupt Stx4 on the PM using IgG-induced crosslinking (Figures S4D and S4E, Movie S5). Whereas Bic/Gly induced exocytosis from recycling endosomes in neurons expressing Stx4-HA, acute application of anti-HA antibody followed by anti-mouse IgG 5 min prior to stimulation significantly reduced postsynaptic exocytosis (Figure 6D). This effect was selective in that application of control anti-Myc antibodies followed by anti-mouse IgG had no effect on activity-induced exocytosis (Figure 6D). Since most Stx4 on the cell surface is complexed in small homo-oligomeric clusters, it is likely that this method disrupts both exogenous Stx4-HA and endogenous Stx4 co-mingled in oligomeric clusters (Low et al., 2006; Sieber et al., 2006). Thus, as with more prolonged manipulations, acute disruption of Stx4 blocks activity-induced exocytosis in dendrites and spines.

We tested if Stx4 mediates the discrete exocytic events we observed in spines by counting the number of spine events over a 20 min time window upon stimulation with Bic/Gly. Disrupting Stx4 function by either expressing Stx4ΔTM or by Stx4 shRNA decreased the number of spine exocytic events nearly three-fold (Figure 6E). Moreover, in accordance with a role in spine RE fusion, blocking Stx4 function led to an accumulation of endosomes in spines (Figures 6F and 6G). These results demonstrate that Stx4 is a central component of the SNARE machinery that mediates rapid, activity-dependent fusion of REs in dendritic spines.

Stx4 Is Required for Long-Term Potentiation in CA1 Hippocampus

To test the physiological consequences of Stx4-dependent cargo insertion on synaptic plasticity, we performed whole cell voltage-clamp recordings of evoked synaptic currents in CA1 pyramidal neurons in acute hippocampal slices. Recombinantly expressed and purified Stx4ΔTM or Stx3ΔTM protein (Figure S5) was acutely introduced into neurons via the recording pipette, and allowed to diffuse into the cytoplasm for 8–10 min following break-in and establishment of whole cell mode. Synaptic strength was monitored every 10 s during this baseline period by recording Schaffer collateral-evoked excitatory postsynaptic currents (EPSCs), after which LTP was induced by depolarizing the cell to 0 mV and delivering 200 stimuli at 2 Hz. Using standard intracellular solution, this induction protocol reliably triggered robust sustained potentiation of EPSC amplitudes to 172 ± 18% of baseline (Figure 7A). However, LTP was almost completely abolished (EPSC amplitudes 111 ± 19% of baseline) when purified Stx4ΔTM (2.5 μM) was included in the recording solution (Figure 7). In contrast, LTP was unaffected (174 ± 15%

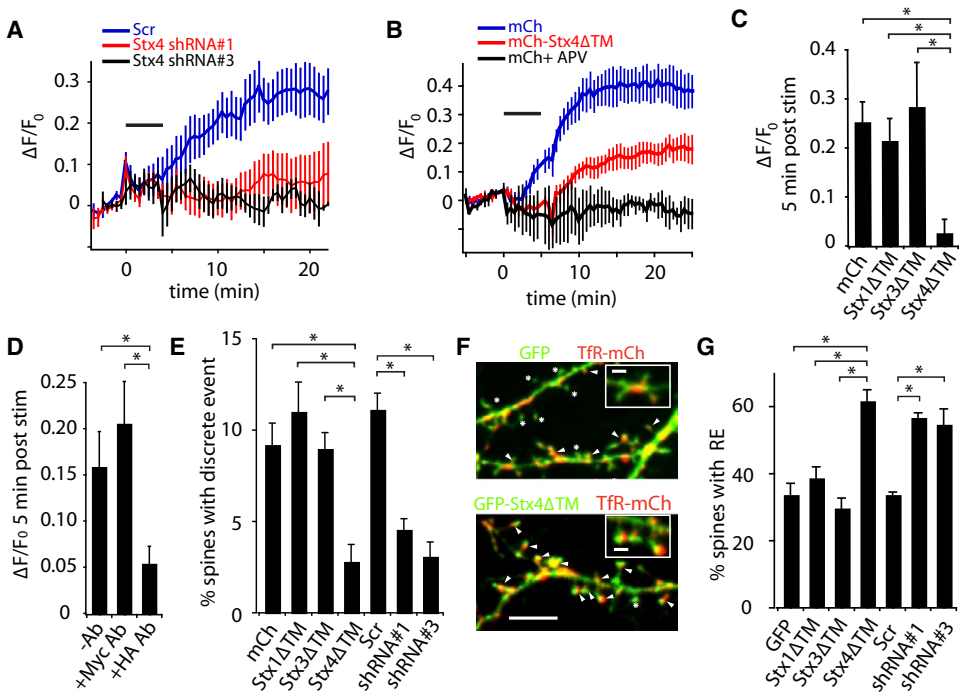

Figure 6. Disrupting Stx4 Inhibits Activity-Triggered Postsynaptic Exocytosis

(A) Stx4 knock down blocks TfR-SEP insertion following stimulation with Bic/Gly. The fractional increase in TfR-SEP fluorescence ($\Delta F/F_0$) was monitored in hippocampal neurons expressing two different shRNAs against Stx4 (shRNA#1, shRNA#3) or a scrambled control shRNA (Scr) along with TfR-SEP. Bic/Gly treatment is indicated by the horizontal bar. Error bars represent SEM. n = 6, 9, 10 for shRNA#1, shRNA#3, and Scr, respectively.

(B) Soluble Stx4 blocks TfR-SEP insertion following stimulation with Bic/Gly. Total TfR-SEP fluorescence was monitored in hippocampal neurons expressing mCh or mCh-Stx4ΔTM. Bic/Gly treatment is indicated by the horizontal bar. Error bars represent SEM. n = 9 cells for each condition.

(C) Postsynaptic exocytosis is blocked by Stx4ΔTM. TfR-SEP insertion was measured on the dendrites of cells expressing mCh, mCh-Stx1ΔTM, mCh-Stx3ΔTM, or mCh-Stx4ΔTM five minutes following stimulation with Bic/Gly. Error bars represent SEM. n = 6, 8, 9, 9 cells respectively, *p < 0.05 Student's t test.

(D) Acute disruption of Stx4 blocks postsynaptic exocytosis. Hippocampal neurons expressing Stx4-HA were incubated with either mouse anti-HA or control anti-Myc antibodies, followed by anti-mouse IgG to acutely crosslink and aggregate Stx4-HA. Error bars represent SEM. n = 7, 6, 9 cells respectively; *p < 0.05, Student's t test.

(E) Stx4 mediates exocytosis in dendritic spines. The total number of TfR-SEP exocytic events in dendritic spines was quantified in hippocampal neurons expressing mCh, mCh-Stx1ΔTM, mCh-Stx3ΔTM, mCh-Stx4ΔTM, Scr shRNA control, Stx4 shRNA#1 or Stx4 shRNA#3 during and 10 min following exposure to Bic/Gly. The total number of spine exocytic events observed during this time period was divided by the total number of spines in the imaged field for each cell. Error bars represent SEM. *p < 0.05, Student's t test, n = 6, 5, 5, 6, 8, 6, 6, cells respectively.

(F) Blocking Stx4 function leads to accumulation of REs in spines. GFP (top panel) or GFP-Stx4ΔTM (bottom panel) was expressed for 48 hr along with TfR-mCh to mark REs in hippocampal neurons. Arrowheads designate RE-positive spines. Asterisks denote endosome-negative spines. The scale bar represents 5 μm; inset, 1 μm.

(G) Quantification of data from (F). Data represent means ± SEM of the percent spines containing a TfR-positive RE in cells expressing GFP, Stx1ΔTM, Stx3ΔTM, Stx4ΔTM, scr shRNA, Stx4 shRNA#1 or Stx4 shRNA#3. *p < 0.05, Student's t test, n = 9, 6, 6, 9, 6, 6, 6, cells respectively. See also Figure S4 and Movie S5.

of baseline) by introduction of purified Stx3ΔTM at an identical concentration, confirming the specificity of the effect. The complete block of LTP (Figure 7) but only partial block of TfR-SEP trafficking (Figure 6B) by Stx4ΔTM may indicate that the early trafficking events (<5 min poststimulation) are more important for LTP since this phase of trafficking was nearly completely blocked by Stx4ΔTM (Figure 6B). These data provide strong evidence that acute postsynaptic block of Stx4 function is sufficient to prevent LTP.

DISCUSSION

In the present study, we employed a novel sensor of postsynaptic membrane trafficking that allowed us to simultaneously visualize the location of exocytosis and the behavior of exocytic cargo prior to, during, and following synaptic activity. We have demonstrated that synaptic activation triggers fusion of large AMPA receptor-containing recycling compartments to the PM of dendritic spines in an all-or-none manner. Spine exocytosis occurs at sites enriched for the SNARE protein Stx4 immediately lateral to the PSD. Accordingly, disruption of Stx4 either acutely or chronically blocks membrane fusion and cargo delivery triggered by synaptic activation and acute inhibition of Stx4 abolishes LTP. Stx4 thus defines a SNARE-based exocytic zone for activity-dependent spine modification required for synaptic plasticity.

A Spine Exocytic Domain

Although a crucial role for postsynaptic exocytosis in synaptic plasticity has long been appreciated (Lledo et al., 1998;

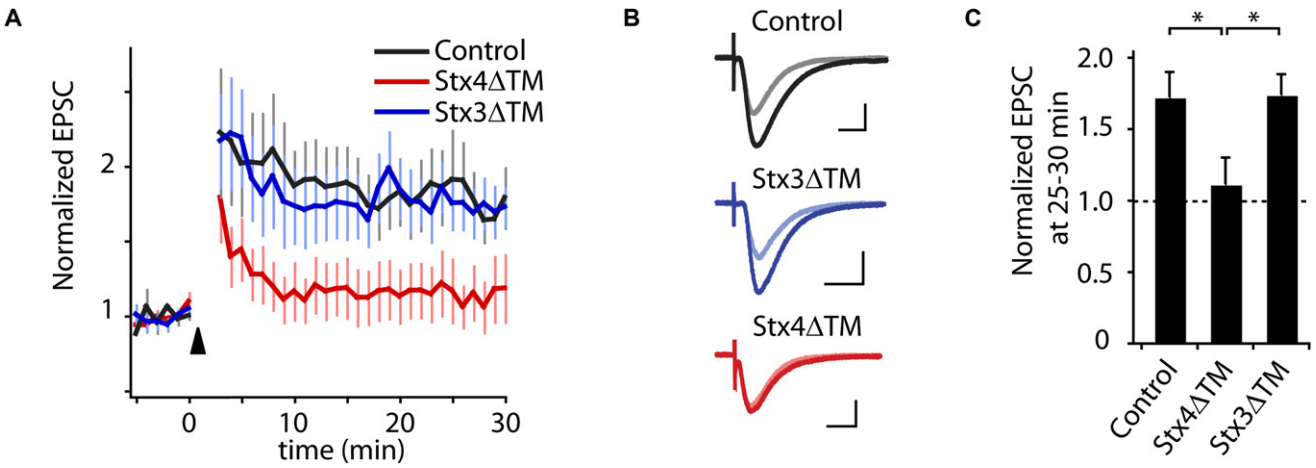

Figure 7. Disrupting Stx4 Blocks LTP

(A) LTP of Schaffer collateral-CA1 synapses was induced by pairing depolarization of the postsynaptic cell to 0 mV with 200 pulses delivered at 2 Hz (arrowhead) with control recording solution (black) or with recording solution containing either 2.5 μm Stx3ΔTM (blue) or Stx4ΔTM (red). Error bars represent SEM n = 7, 8, 8 cells, respectively.

(B) Average of 10 individual EPSCs from representative recordings before pairing (light traces) and 25 min after LTP induction (dark traces) for control, Stx4ΔTM, and Stx3ΔTM conditions. The scale bar represents 50 pA, 25 msec.

(C) Bar graph summarizing the effect of StxΔTM peptides on the magnitude of LTP at 25-30 min. LTP was nearly abolished by Stx4ΔTM (*$p < 0.05$ relative to control), but was unaffected by Stx3ΔTM ($p > 0.9$ relative to control). See also Figure S5.

Lu et al., 2001; Luscher et al., 1999; Yoshihara et al., 2005), the site(s) of membrane insertion has been unknown and controversial. Recent studies have suggested that activity stimulates exocytosis of synaptic cargo exclusively in the soma and dendritic shafts (Adesnik et al., 2005; Makino and Malinow, 2009; Yudowski et al., 2007), while others support a more local trafficking pathway within activated dendritic spines (Gerges et al., 2006; Kopec et al., 2006; Park et al., 2006). Here, we provide direct evidence for activity-regulated exocytic trafficking within dendritic spines. Upon stimulation, intra-spine endosomes undergo abrupt fusion with the spine PM. Prior to fusion, spine-localized endosomes load with endogenous GluR1 and exogenous transferrin, indicating that these structures participate in ongoing recycling of plasma membrane proteins, including neurotransmitter receptors. Importantly, we show that, relative to endogenous GluR1, exogenously expressed SEP-GluR1 traffics less efficiently through spine REs. Specifically, less than half of spine REs contain SEP-GluR1 compared to nearly complete labeling of spine REs after endogenous GluR1 antibody feeding. This could be due to incomplete stoichiometric association with AMPA receptor regulatory subunits (e.g., TARPS), and may explain differences between our results and studies that failed to observe spine exocytosis using SEP-GluR1 (Makino and Malinow, 2009; Yudowski et al., 2007).

Our results indicate that spine-localized recycling endosomes sense synaptic activity and rapidly alter the composition of the spine PM in dramatic, presumably single-step exocytic events at sites adjacent to the PSD. The location of exocytosis adjacent to the PSD indicates that incorporation of newly exocytosed membrane proteins into the PSD will be limited by escape and lateral diffusion from the initial site of fusion. The spine neck sequesters newly inserted material within the spine head for tens of seconds, increasing the likelihood of synaptic incorporation and perhaps shielding unstimulated neighboring synapses from newly inserted plasticity factors. Thus, while exocytic trafficking may be necessary for synaptic plasticity, short-range diffusion to the PSD within the confines of the spine head will likewise limit the rate and range of cargo incorporation into the synapse (Holcman and Triller, 2006; Newpher and Ehlers, 2008; Triller and Choquet, 2008; Yang et al., 2008a). Intriguingly, at many spines, the fraction of newly inserted SEP-GluR1 remains nearly constant for several minutes following exocytosis, even though co-exocytosed TfR-mCh quickly diffuse away. Although measuring spine exocytosis following more refined activity manipulations will be required to directly link spine exocytosis with homosynaptic LTP, this quantal mode of incorporation of AMPA receptors mirrors the single-step potentiation of AMPA receptor currents reported at individual synapses following local glutamate uncaging or weak afferent stimulation (Bagal et al., 2005; Makino and Malinow, 2009; Matsuzaki et al., 2004; O'Connor et al., 2005; Petersen et al., 1998). In particular, both events are NMDA receptor-dependent, occur in a "digital" all-or-none fashion, and are refractory to further stimulation. A possible mechanism that could set the refractory period for additional potentiation is the genesis of new spine REs or the mobilization existing REs into spines, the latter of which involves myosin Vb-mediated translocation of dendritic endosomes into spines (Wang et al., 2008).

A Postsynaptic Syntaxin

We have found that Stx4, a PM SNARE protein expressed in brain, mediates a majority of activity-triggered membrane trafficking events from postsynaptic recycling compartments. Stx4 localizes to dendritic spines where it marks sites where spine

endosomes fuse with the spine PM, thus enabling synapse-specific membrane delivery. In concert with previously described endocytic zones (Blanpied et al., 2002; Lu et al., 2007; Racz et al., 2004), the discovery of spine exocytic machinery raises the intriguing possibility of a micron-scale membrane trafficking circuit that determines the unique properties of individual synapses. Indeed, disrupting this circuit by eliminating postsynaptic endocytic zones results in loss of synaptic AMPA receptors, loss of local AMPA receptor recycling, and impaired synaptic potentiation (Lu et al., 2007; Petrini et al., 2009). Here we have shown that recycling cargo, including AMPA receptors can be exocytosed directly in spines, indicating that both exocytosis and endocytosis can be spatially restricted on a micron scale. In addition to AMPA receptors, many other postsynaptic membrane proteins are known to traffic through recycling endosomal compartments, including N-cadherin, L-type voltage-gated calcium channels, A-type potassium channels and metabotropic glutamate receptors. Likewise, soluble factors, including neurotrophins, may also be released via spine exocytosis (Dean et al., 2009). Although further experiments are needed to reveal the complete array of factors trafficked through spine endosomes and exocytosed at Stx4 exocytic domains, we speculate that these organelles act as input-specific, activity-triggered plasticity modules that harbor and deliver a variety of membrane and secreted factors that modify diverse features of glutamatergic synapses. Further, it is interesting to note that unlike the classic presynaptic syntaxin Stx1, Stx4 associates with and is tightly regulated by the actin cytoskeleton (Jewell et al., 2008; Low et al., 2006), an adaptation particularly suited for actin-rich dendritic spines. Ultimately, spatially directed exocytosis together with retention of receptors and other exocytic cargo in the PSD, could both acutely augment and persistently confine new components of a given synapse for enduring changes in synaptic strength. More broadly, localized Stx4 exocytic domains may provide a general paradigm for stimulus-dependent regulation of local membrane composition on a micron scale.

EXPERIMENTAL PROCEDURES

Cell Culture and Transfection

Hippocampal neuron cultures were prepared from E18 rat embryos and grown on 18 mm poly-D-lysine coated coverslips as previously described (Ehlers, 2000). COS7 cells were grown in DMEM supplemented with 10% fetal bovine serum. Cells were transfected using Lipofectamine 2000 (Invitrogen) according to the manufacturer's recommendations.

Live Cell Imaging

Live cell imaging was performed on a custom built spinning disc confocal microscope with a Yokogawa CSU10 scan head mounted on a Nikon TE300 inverted stand. Excitation was provided by a 2.5W KrAr laser (SpectraPhysics).

Antibody and Transferrin Labeling of Live Cells

For live-cell surface labeling of Stx4-HA, cells were washed with imaging buffer and incubated for 3 min with mouse monoclonal anti-HA.11 antibody (Covance 16B12) at 32°C. For live-cell antibody feeding experiments, hippocampal neurons (DIV 20-25) transfected with GFP and TfR-mCh were incubated for 3 hr at 37°C with 0.75 μg/mL affinity-purified anti-GluR1 antibody directed against the extracellular N-terminal domain. For transferrin loading experiments, cells were incubated for 30 min in serum free media supplemented with 50 μg/mL Alexa 647-conjugated transferrin (Molecular Probes/Invitrogen).

Immunogold Electron Microscopy

Immunogold electron microscopy was performed on ultramicrotome sections of adult rat CA1 hippocampus as previously described (Park et al., 2006; Racz et al., 2004).

Generation of Recombinant Stx3ΔTM and Stx4ΔTM

Recombinant Stx4ΔTM and Stx3ΔTM were generated as N-terminal GST fusion proteins by cloning sequences corresponding to amino acids 2–273 of human Stx4 and amino acids 2-262 of Stx3 into pGEX-6P-3 (Amersham Biosciences). GST-StxΔTM proteins were produced in *E. coli* strain BL21(DE3) pLysS after a 4 hr induction with 1 mM IPTG at room temperature and purified over glutathione sepharose 4B resin. To prepare recording solutions containing Stx protein, 1 ml of recombinantly expressed StxΔTM protein was dialyzed overnight against 2 × 1L of (in mM): 115 cesium methane sulfonate, 20 $CsCl_2$, 10 HEPES (pH 7.3).

Electrophysiology

LTP experiments were performed using transverse hippocampal slices cut from C57Bl/6 mice (350 μm, ~3 weeks of age, Charles River). Whole cell voltage clamp recordings were made from CA1 pyramidal neurons using IR-DIC optics with internal solutions supplemented with 2.5 μM Stx4ΔTM or Stx3ΔTM. All recordings were blind with respect to the identity of the recombinant protein. Schaffer collaterals were activated at 0.1 Hz using a bipolar stainless steel stimulating electrode (50–200 μA, 100 μsec) and monosynaptic EPSCs were measured at −70 mV. Cells were dialyzed for 9–10 min to allow peptide diffusion, before inducing LTP by pairing depolarization to 0 mV with 200 stimuli at 2 Hz.

SUPPLEMENTAL INFORMATION

Supplemental Information includes Extended Experimental Procedures, five figures, and five movies and can be found with this article online at doi:10.1016/j.cell.2010.02.042.

ACKNOWLEDGMENTS

We thank Marguerita Klein, Irina Lebedeva, and Haiwei Zhang for excellent technical assistance. We thank Ben Arenkiel, Cyril Hanus, Juliet Hernandez, Tom Newpher, Michael Patterson, Joel Schwartz, Chandra Tucker, Ryohei Yasuda, and Richard Weinberg for critical discussion and review of this manuscript. This work was supported by grants from NIMH, NINDS, and NIA to M.D.E. M.D.E. is an Investigator of the Howard Hughes Medical Institute.

Received: March 2, 2009
Revised: December 10, 2009
Accepted: February 22, 2010
Published: April 29, 2010

REFERENCES

Adesnik, H., Nicoll, R.A., and England, P.M. (2005). Photoinactivation of native AMPA receptors reveals their real-time trafficking. Neuron *48*, 977–985.

Ashby, M.C., Maier, S.R., Nishimune, A., and Henley, J.M. (2006). Lateral diffusion drives constitutive exchange of AMPA receptors at dendritic spines and is regulated by spine morphology. J. Neurosci. *26*, 7046–7055.

Bagal, A.A., Kao, J.P., Tang, C.M., and Thompson, S.M. (2005). Long-term potentiation of exogenous glutamate responses at single dendritic spines. Proc. Natl. Acad. Sci. USA *102*, 14434–14439.

Blanpied, T.A., Scott, D.B., and Ehlers, M.D. (2002). Dynamics and regulation of clathrin coats at specialized endocytic zones of dendrites and spines. Neuron *36*, 435–449.

Dean, C., Liu, H., Dunning, F.M., Chang, P.Y., Jackson, M.B., and Chapman, E.R. (2009). Synaptotagmin-IV modulates synaptic function and long-term potentiation by regulating BDNF release. Nat. Neurosci. *12*, 767–776.

Ehlers, M.D. (2000). Reinsertion or degradation of AMPA receptors determined by activity-dependent endocytic sorting. Neuron *28*, 511–525.

Gerges, N.Z., Backos, D.S., Rupasinghe, C.N., Spaller, M.R., and Esteban, J.A. (2006). Dual role of the exocyst in AMPA receptor targeting and insertion into the postsynaptic membrane. EMBO J. *25*, 1623–1634.

Holcman, D., and Triller, A. (2006). Modeling synaptic dynamics driven by receptor lateral diffusion. Biophys. J. *91*, 2405–2415.

Jahn, R., and Scheller, R.H. (2006). SNAREs–engines for membrane fusion. Nat. Rev. Mol. Cell Biol. *7*, 631–643.

Jewell, J.L., Luo, W., Oh, E., Wang, Z., and Thurmond, D.C. (2008). Filamentous actin regulates insulin exocytosis through direct interaction with Syntaxin 4. J. Biol. Chem. *283*, 10716–10726.

Kennedy, M.J., and Ehlers, M.D. (2006). Organelles and trafficking machinery for postsynaptic plasticity. Annu. Rev. Neurosci. *29*, 325–362.

Kopec, C.D., Li, B., Wei, W., Boehm, J., and Malinow, R. (2006). Glutamate receptor exocytosis and spine enlargement during chemically induced long-term potentiation. J. Neurosci. *26*, 2000–2009.

Kopec, C.D., Real, E., Kessels, H.W., and Malinow, R. (2007). GluR1 links structural and functional plasticity at excitatory synapses. J. Neurosci. *27*, 13706–13718.

Lang, T., Bruns, D., Wenzel, D., Riedel, D., Holroyd, P., Thiele, C., and Jahn, R. (2001). SNAREs are concentrated in cholesterol-dependent clusters that define docking and fusion sites for exocytosis. EMBO J. *20*, 2202–2213.

Lledo, P.M., Zhang, X., Sudhof, T.C., Malenka, R.C., and Nicoll, R.A. (1998). Postsynaptic membrane fusion and long-term potentiation. Science *279*, 399–403.

Low, S.H., Vasanji, A., Nanduri, J., He, M., Sharma, N., Koo, M., Drazba, J., and Weimbs, T. (2006). Syntaxins 3 and 4 are concentrated in separate clusters on the plasma membrane before the establishment of cell polarity. Mol. Biol. Cell *17*, 977–989.

Lu, J., Helton, T.D., Blanpied, T.A., Racz, B., Newpher, T.M., Weinberg, R.J., and Ehlers, M.D. (2007). Postsynaptic positioning of endocytic zones and AMPA receptor cycling by physical coupling of dynamin-3 to Homer. Neuron *55*, 874–889.

Lu, W., Man, H., Ju, W., Trimble, W.S., MacDonald, J.F., and Wang, Y.T. (2001). Activation of synaptic NMDA receptors induces membrane insertion of new AMPA receptors and LTP in cultured hippocampal neurons. Neuron *29*, 243–254.

Luscher, C., Xia, H., Beattie, E.C., Carroll, R.C., von Zastrow, M., Malenka, R.C., and Nicoll, R.A. (1999). Role of AMPA receptor cycling in synaptic transmission and plasticity. Neuron *24*, 649–658.

Makino, H., and Malinow, R. (2009). AMPA receptor incorporation into synapses during LTP: the role of lateral movement and exocytosis. Neuron *64*, 381–390.

Maletic-Savatic, M., and Malinow, R. (1998). Calcium-evoked dendritic exocytosis in cultured hippocampal neurons. Part I: trans-Golgi network-derived organelles undergo regulated exocytosis. J. Neurosci. *18*, 6803–6813.

Martens, S., and McMahon, H.T. (2008). Mechanisms of membrane fusion: disparate players and common principles. Nat. Rev. Mol. Cell Biol. *9*, 543–556.

Matsuzaki, M., Honkura, N., Ellis-Davies, G.C., and Kasai, H. (2004). Structural basis of long-term potentiation in single dendritic spines. Nature *429*, 761–766.

Miesenbock, G., De Angelis, D.A., and Rothman, J.E. (1998). Visualizing secretion and synaptic transmission with pH-sensitive green fluorescent proteins. Nature *394*, 192–195.

Newpher, T.M., and Ehlers, M.D. (2008). Glutamate receptor dynamics in dendritic microdomains. Neuron *58*, 472–497.

O'Connor, D.H., Wittenberg, G.M., and Wang, S.S. (2005). Graded bidirectional synaptic plasticity is composed of switch-like unitary events. Proc. Natl. Acad. Sci. USA *102*, 9679–9684.

Ohara-Imaizumi, M., Nishiwaki, C., Kikuta, T., Kumakura, K., Nakamichi, Y., and Nagamatsu, S. (2004). Site of docking and fusion of insulin secretory granules in live MIN6 beta cells analyzed by TAT-conjugated anti-syntaxin 1 antibody and total internal reflection fluorescence microscopy. J. Biol. Chem. *279*, 8403–8408.

Olson, A.L., Knight, J.B., and Pessin, J.E. (1997). Syntaxin 4, VAMP2, and/or VAMP3/cellubrevin are functional target membrane and vesicle SNAP receptors for insulin-stimulated GLUT4 translocation in adipocytes. Mol. Cell. Biol. *17*, 2425–2435.

Park, M., Penick, E.C., Edwards, J.G., Kauer, J.A., and Ehlers, M.D. (2004). Recycling endosomes supply AMPA receptors for LTP. Science *305*, 1972–1975.

Park, M., Salgado, J.M., Ostroff, L., Helton, T.D., Robinson, C.G., Harris, K.M., and Ehlers, M.D. (2006). Plasticity-induced growth of dendritic spines by exocytic trafficking from recycling endosomes. Neuron *52*, 817–830.

Passafaro, M., Piech, V., and Sheng, M. (2001). Subunit-specific temporal and spatial patterns of AMPA receptor exocytosis in hippocampal neurons. Nat. Neurosci. *4*, 917–926.

Petersen, C.C., Malenka, R.C., Nicoll, R.A., and Hopfield, J.J. (1998). All-or-none potentiation at CA3-CA1 synapses. Proc. Natl. Acad. Sci. USA *95*, 4732–4737.

Petrini, E.M., Lu, J., Cognet, L., Lounis, B., Ehlers, M.D., and Choquet, D. (2009). Endocytic trafficking and recycling maintain a pool of mobile surface AMPA receptors required for synaptic potentiation. Neuron *63*, 92–105.

Racz, B., Blanpied, T.A., Ehlers, M.D., and Weinberg, R.J. (2004). Lateral organization of endocytic machinery in dendritic spines. Nat. Neurosci. *7*, 917–918.

Shepherd, J.D., and Huganir, R.L. (2007). The cell biology of synaptic plasticity: AMPA receptor trafficking. Annu. Rev. Cell Dev. Biol. *23*, 613–643.

Sieber, J.J., Willig, K.I., Heintzmann, R., Hell, S.W., and Lang, T. (2006). The SNARE motif is essential for the formation of syntaxin clusters in the plasma membrane. Biophys. J. *90*, 2843–2851.

Sieber, J.J., Willig, K.I., Kutzner, C., Gerding-Reimers, C., Harke, B., Donnert, G., Rammner, B., Eggeling, C., Hell, S.W., Grubmuller, H., et al. (2007). Anatomy and dynamics of a supramolecular membrane protein cluster. Science *317*, 1072–1076.

Sollner, T., Bennett, M.K., Whiteheart, S.W., Scheller, R.H., and Rothman, J.E. (1993). A protein assembly-disassembly pathway in vitro that may correspond to sequential steps of synaptic vesicle docking, activation, and fusion. Cell *75*, 409–418.

Takamori, S., Holt, M., Stenius, K., Lemke, E.A., Gronborg, M., Riedel, D., Urlaub, H., Schenck, S., Brugger, B., Ringler, P., et al. (2006). Molecular anatomy of a trafficking organelle. Cell *127*, 831–846.

Tanaka, J., Horiike, Y., Matsuzaki, M., Miyazaki, T., Ellis-Davies, G.C., and Kasai, H. (2008). Protein synthesis and neurotrophin-dependent structural plasticity of single dendritic spines. Science *319*, 1683–1687.

Triller, A., and Choquet, D. (2008). New concepts in synaptic biology derived from single-molecule imaging. Neuron *59*, 359–374.

Wang, Z., Edwards, J.G., Riley, N., Provance, D.W., Jr., Karcher, R., Li, X.D., Davison, I.G., Ikebe, M., Mercer, J.A., Kauer, J.A., et al. (2008). Myosin Vb mobilizes recycling endosomes and AMPA receptors for postsynaptic plasticity. Cell *135*, 535–548.

Yang, Y., Wang, X.B., Frerking, M., and Zhou, Q. (2008a). Delivery of AMPA receptors to perisynaptic sites precedes the full expression of long-term potentiation. Proc. Natl. Acad. Sci. USA *105*, 11388–11393.

Yang, Y., Wang, X.B., Frerking, M., and Zhou, Q. (2008b). Spine expansion and stabilization associated with long-term potentiation. J. Neurosci. *28*, 5740–5751.

Yoshihara, M., Adolfsen, B., Galle, K.T., and Littleton, J.T. (2005). Retrograde signaling by Syt 4 induces presynaptic release and synapse-specific growth. Science *310*, 858–863.

Yudowski, G.A., Puthenveedu, M.A., Leonoudakis, D., Panicker, S., Thorn, K.S., Beattie, E.C., and von Zastrow, M. (2007). Real-time imaging of discrete exocytic events mediating surface delivery of AMPA receptors. J. Neurosci. *27*, 11112–11121.

Cell

EXTENDED EXPERIMENTAL PROCEDURES

Constructs

TfR-SEP was previously described (Park et al., 2006). Human Stx4 and Stx3 clones were provided by Dr. Thomas Weimbs (University of California, Santa Barbara). Stx1a was from Genecopoeia. Stx4-HA was generated by cloning the Stx4 coding sequence into a custom mammalian expression vector containing CMV promoter elements and a C-terminal HA sequence. mCherry-Stx4ΔTM and mCherry-Stx3ΔTM were generated by PCR amplification and subcloning of the sequences encoding amino acids 2–273 (Stx4), 2–263 (Stx3), and 2–265 (Stx1) into the mCherry-N1 vector, a gift from Dr. Roger Tsien (University of California, San Diego). GST-Stx4ΔTM and GST-Stx3ΔTM were generated by PCR amplification and subcloning of the sequences encoding amino acids 2–273 (Stx4) or amino acids 2–263 (Stx3) into pGEX-6P-3. TfR-mCh-SEP was generated by cloning a PCR-generated mCh fragment into an AgeI site in TfR-SEP (Park et al., 2006). GFP-homer1c was provided by Dr. Daniel Choquet (University of Bordeaux). SEP-GluR1 was generated from a GFP-GluR1 construct provided by Dr. Richard Huganir (Johns Hopkins University).

shRNA Knockdown of Stx4

For shRNA knockdown of Stx4, we used the following 19-mer target sequences: Stx4shRNA#1: AGACAATTCGGCAGACTAT; Stx4shRNA#3: CCTGCGAGAGGAGATCAAA. The DNA oligonucleotides containing the shRNA target sequence, a 9 nucleotide loop region (TTCAAGAGA), and the shRNA antisense sequence were ligated and cloned into pLentilox3.7 (a gift from Dr. Tyler Jacks) modified to express tdTomato as a cell fill. pLentilox3.7 expressing a scrambled shRNA sequence was used as a negative control. To verify the efficacy of our shRNA sequences, we infected NIH 3T3 cells or hippocampal neuron cultures at DIV 0-3 with lentivirus packaged with pLentilox3.7 harboring either scrambled control shRNA or shRNA targeting Stx4. Cell lysates were collected 4–5 days later for immunoblot analysis. For imaging TfR-SEP insertion, neurons were transfected with pLentilox3.7 plus TfR-SEP constructs at DIV 13 and imaged 4–5 days later (DIV 17-18).

Live Cell Imaging

Live cell imaging was performed on a custom built spinning disc confocal microscope with a Yokogawa CSU10 scan head mounted on a Nikon TE300 inverted stand. Excitation was provided by a 2.5W KrAr laser (SpectraPhysics) shuttered via an acousto-optical tunable filter (AOTF) (Neos Technologies), with emission directed through a filter wheel (Applied Scientific Instrumentation) holding either band pass or long pass filters (Chroma). Images were acquired using a 60× Plan Apochromat 1.4 NA objective. A 1.5× tube lens between the filter wheel and camera focused light on the chip of a Hamamatsu C9100 EM-CCD camera giving a pixel size of 86 × 86 nm. The focal plane was controlled by a piezo-driven Z-stage (Applied Scientific Instruments). The EM-CCD Camera, filter wheel, stage, and AOTF laser line switching were controlled by Metamorph software (Molecular Devices). Chromatic aberration between red and green channels was evaluated by imaging dual color Focalcheck microspheres (Invitrogen) and was found to be minimal. An environmental chamber (In Vivo Scientific) enclosing the microscope stand maintained the temperature at 37°C. In some experiments, images were acquired on a Perkin Elmer Ultraview spinning disc system equipped with a 60x Plan Apochromat 1.4 NA objective.

Between 24–48 hr following transfection, coverslips (Deckgläser #1, 18 mm) with cultured hippocampal neurons were placed in a live cell imaging chamber (Ludin) and perfused with media containing (in mM): 130 NaCl, 5 KCl, 2 $CaCl_2$, 10 HEPES, 30 glucose, and 1 $MgCl_2$, (pH 7.4). Neurons were stimulated by exchanging the above solution to one that contained (in mM): 130 NaCl, 5 KCl, 10 HEPES, 30 glucose, 3 $CaCl_2$, 0.03 (-) bicuculline methiodide (Tocris), 0.2 Glycine (Tocris), pH 7.4 (Bic/Gly solution). Neurons were incubated in Bic/Gly solution for 5 min before being returned to extracellular solution. Stacks of images were acquired before, during, and following stimulation with spacing of 0.5 μm in the z-axis, except in cases where rapid acquisition was necessary, in which case images were captured in a single image plane.

For experiments monitoring the ratio of the mCh and SEP signal of TfR-mCh-SEP, the intrinsic ratio of mCh to SEP signal was determined at neutral pH by incubating neurons in NH_4Cl (50 mM) and acquiring red (mCh) and green (SEP) signal. The value obtained (mCh/SEP_{neut}) is an arbitrary constant that depends on imaging conditions (EM-CCD gain, laser intensity, integration time). Provided imaging conditions are kept constant, mCh/SEP values provide a measure of the fraction of TfR-mCh-SEP molecules present in an acidic endosomes. For timelapse imaging of mCh/SEP_{neut} during exocytosis, we corrected for the pre-exocytosis bleaching of mCh (during which time SEP was protected from bleaching in acidic endosomes) by fitting the total cellular mCh signal to a single exponential and calculating the fractional mCh signal bleached during the pre-exocytosis imaging period. For visualization, some images were low pass filtered and interpolated. Only raw data was used for quantification.

Antibody and Transferrin Labeling of Live Cells

For live-cell surface labeling of Stx4-HA, cells were washed with imaging buffer and incubated for 3 min with mouse monoclonal anti-HA.11 antibody (Covance 16B12) at 32°C. Coverslips were then washed and incubated for 3-4 min with goat anti-mouse F_{ab} conjugated to Cy3 (Jackson Immunologicals) or Alexa 647 (Molecular Probes/Invitrogen) at 32°C. Imaging commenced immediately following washout of the dye-conjugated secondary antibody. Only cells with a minimal detectable level of surface labeling were imaged as we observed very few exocytic events when Stx4 was expressed at high levels. As a control, cells were fixed prior to labeling under nonpermeabilizing conditions to confirm that the punctate pattern of surface Stx4 was not a consequence of

antibody-induced clustering in live cells. For antibody-induced disruption of surface Stx4 in live cells, the same protocol outlined above was followed except that anti-mouse whole IgG was used instead of anti-mouse F_{ab} secondary antibodies. Labeling in this manner rapidly (<5 min) induced large, immobile Stx4-HA aggregates at the PM.

For transferrin loading experiments, cells were incubated for 30 min in serum free media supplemented with 50 μg/mL Alexa 647-conjugated transferrin (Molecular Probes/Invitrogen). Cells were washed with imaging buffer prior to visualization.

For live-cell antibody feeding experiments, hippocampal neurons (DIV 20-25) transfected with GFP and TfR-mCh were incubated for 3 hr at 37°C with 0.75 μg/mL affinity-purified anti-GluR1 antibody directed against the extracellular N-terminal domain. Cells were washed with PBS and fixed with 4% paraformaldehyde for 20 min at room temperature. Cells were blocked overnight with 0.5 mg/mL anti-rabbit F_{ab} (Jackson Immunologicals) in PBS. Following block, cells were permeabilized with 0.1% Triton X-100 and labeled with Alexa 647-conjugated anti-rabbit secondary for 1 hr. Nonpermeabilized cells were used to control for surface anti-GluR1 blocking efficiency. To control for nonspecific uptake of anti-GluR1, we preincubated the antibody with a 10-fold molar excess of the peptide used to generate the antibody.

Image Analysis

To quantify total TfR-SEP insertion into dendrites and spines, the initial fluorescence (F_0) after background correction was subtracted from the fluorescence at subsequent time points during and after Bic/Gly stimulation and divided by F_0 to obtain the fractional increase in TfR-SEP fluorescence according to the relation $(F_t - F_0)/F_0$. Quantification was performed on two-dimensional projections of z-stacks acquired at each time point. Only dendrites and spines were included in the analysis. For centroid analysis, relevant regions were fit using Igor Pro software (Wavemetrics) with the 2-dimensional Gaussian function

$$f(x,y) = z_0 + Ae^{-\left(\frac{(x-x_0)^2}{2\sigma_x^2} + \frac{(y-y_0)^2}{2\sigma_y^2}\right)}$$

where z_0 is the baseline offset, A is the maximum amplitude, x_0 and y_0 are the center in the x and y dimensions, and $\sigma_{x,y}$ is the width of the function in the x and y dimension. Cell boundaries were designated by thresholding the cell-fill (or in some cases TfR-SEP or TfR-mCh) channel (typically at 10% over background), and outlining the cell.

Immunohistochemistry

For syntaxin labeling in brain sections, C57BL/6 mice (P20-P30) were perfused with 10 ml PBS followed by 10 ml 4% PFA in PBS. Brains were dissected and postfixed for 1 hr at 4°C in 4% PFA in PBS. Brains were frozen in O.C.T (Tissue-Tek) and 50 μm coronal sections were cut on a Microm HM400 microtome. Sections were permeabilized and blocked in PBS containing 0.1% Triton X-100, 3% BSA, and 10% normal goat serum for 12 hr at 4°C. Sections were washed three times with PBS containing 0.1% Triton X-100 before application of antibodies. Primary antibodies were diluted in blocking solution and incubated with sections for at least 12 hr at 4°C before washing 3 times in PBS with 0.1% Triton X-100. Secondary antibodies were also diluted in the blocking solution and incubated with sections for at least 6 hr. Following antibody application, slices were washed extensively prior to mounting onto microscope slides using Vectashield mountant (Vector Laboratories).

For antibody staining of cultured neurons, cells grown on glass coverslips were fixed in 4% PFA in PBS for 20 min at room temperature. Coverslips were then washed in PBS before permeabilizing and blocking for 1 hr at room temperature with PBS containing 0.1% Triton X-100, 3% BSA, and 10% normal goat serum. Primary antibodies were diluted in blocking solution and added to coverslips for at least 1 hr before washing three times in PBS with 0.1% Triton X-100. Secondary antibodies were also diluted in blocking solution and added to coverslips for at least 1 hr. Following antibody application, cells were washed extensively prior to mounting onto microscope slides using Permafluor mountant containing 50 mg/mL 1,4-diazabicyclo[2.2.2]octane (Sigma).

Two anti-Stx4 antibodies were used in this study: Chemicon AB5330 and Sigma S9924. Both antibodies were used at 1:400 for brain sections and 1:250 for cultured hippocampal neurons. Alexa488, 568, or 647-conjugated goat anti-rabbit secondary antibodies (Molecular Probes/Invitrogen) were used at 1:500 dilution. As a control for Stx4 antibody staining, we preincubated anti-Stx4 with a 10-fold molar excess of the peptide antigen used to generate the antibody (amino acids 2-23) for 1 hr at room temperature prior to staining. Preincubation with the antigenic peptide blocked all Stx4 staining in both cultured neurons and in brain slices.

Immunogold Electron Microscopy

Deeply anesthetized male Sprague-Dawley rats were perfused with saline followed by cold fixative, containing 4% paraformaldehyde and 0.1% glutaraldehyde in phosphate buffer (PB, 0.1M, [pH 7.4]). Brains were removed and postfixed in the same fixative for 2 hr. Coronal sections (50 μm thick) were cut with a Vibratome, and then washed in PB. For pre-embedding immunolabeling, floating sections were washed in phosphate buffered saline (PBS, 0.01 M, [pH 7.4]) and treated for 30 min in 1% sodium borohydride in PBS, washed in PBS, treated with 3% H_2O_2 in PBS, and washed again in PBS. Sections were then incubated in 20% normal donkey serum (NDS, Jackson ImmunoResearch) for 30 min, and overnight in rabbit anti-syntaxin 4 (Sigma), mouse anti-syntaxin 1 (Synaptic Systems), rabbit anti-syntaxin 2 (Synaptic Systems) or rabbit anti-syntaxin 3 (Synaptic Systems) in PBS containing 2% NDS. Following several washes in PBS and incubation in PBS containing 2% NDS, sections were incubated in biotinylated

donkey anti-rabbit or mouse IgG (1:200, Jackson ImmunoResearch Laboratories Inc.) for 2 hr, washed with PBS, incubated with 1.4 nm gold particles conjugated to streptavidin (Nanoprobes) diluted 1:100 in PBS for 2 hr, and washed with PBS. Following gold labeling, sections were fixed with 1% glutaraldehyde (Electron Microscopy Sciences) in PBS for 10 min and washed in PBS. Gold particle labeling was enhanced using IntenseS-EM (Amersham) after washing in 0.05 M sodium acetate. Following enhancement, sections were washed in sodium acetate and PB and were then postfixed with 1% OsO_4 in PB for 45 min, washed in PB, washed in maleate buffer (0.1 M), contrasted in 1% uranyl acetate in maleate buffer for 45 min, and washed in maleate buffer prior to dehydration in a graded series of ethanol washes. Ethanol was replaced by propylene oxide (Electron Microscopy Sciences) and the tissue was infiltrated with dilutions (50%–100%) of Epon-Spurr's resin (6:4; Electron Microscopy Sciences) in propylene oxide over three hours. For postembedding immunolabeling, tissue was prepared as in Phend et al., 1995 with minor modifications. Briefly, tissue was washed in 0.1M sodium acetate, incubated in 1% tannic acid in sodium acetate, and washed again in sodium acetate. Following incubation in 0.1% calcium chloride and 0.005% zinc acetate in sodium acetate, tissue was stained *en bloc* with 1% uranyl acetate in sodium acetate. Sections were dehydrated in a graded series of ethanol washes and infiltrated with dilutions (50%–100%) of Spurr's resin in ethanol. For all tissues, sections were sandwiched between ACLAR films (Ted Pella) following infiltration, flattened between microscope slides, and polymerized at 60°C for 48 hr. Samples from the area of interest (CA1) were removed and fixed to resin blocks for thin sectioning. Thin sections (~60 nm) were cut on a Leica ultramicrotome and collected on copper grids. Grids were contrasted with uranyl acetate and Sato's lead and examined in a Philips Tecnai electron microscope at 80 kV. Digital micrographs were acquired with a 16-bit FEI Eagle 2048 × 2048 CCD camera. Images were converted to 8-bit files and cropped using ImageJ (Rasband, W.S., ImageJ, U. S. National Institutes of Health, Bethesda, Maryland, USA, http://rsb.info.nih.gov/ij/, 1997–2008.)

For postembedding immunolabeling, thin sections on nickel grids were blocked in 50 mM glycine in 10 mM PBS and then in serum blocking solution specific to the secondary antibody (Aurion/Electron Microscopy Sciences). Sections were equilibrated in 0.1% BSA-c (Aurion/Electron Microscopy Sciences) and stained overnight with primary antibody at 4°C. Following primary antibody incubation, sections were extensively washed with BSA-c/PBS buffer and incubated with 10 nm gold conjugated to $F(ab')_2$ fragments of goat anti-rabbit antibodies (Aurion/Electron Microscopy Sciences) diluted in BSA-c/PBS for 2 hr at room temperature. Grids were then extensively washed in BSA-c/PBS and PBS alone and then fixed in 2% glutaraldehyde in PBS. Following fixation, grids were washed with PBS and water then contrasted and viewed as above.

For quantification, distance measurements were made perpendicular from the long axis of the PSD to a parallel plane bisecting the immunogold label (Figure S4A). For normalized tangential distances, the distance around the periphery of the spine head was measured from one side of the PSD to the immunogold label and from the immunogold label back to the second edge of the PSD. Only immunogold labels that were touching the membrane were measured for tangential distance. When an open spine neck was encountered in the peripheral distance measurement, the spine was 'closed' at the narrowest point of the neck, crossing it in the manner most perpendicular to the membranes. The normalized tangential distance is expressed as a relative distance from 0 to 1 where 0 represents the edge of the PSD and 1 represents the point in the spine farthest from the PSD. The labeling frequency was calculated as a 2-bin (100 nm bins) running average and then normalized. All measurements were taken using ImageJ.

Generation of Recombinant Stx3ΔTM and Stx4ΔTM

Recombinant Stx4ΔTM and Stx3ΔTM were generated as N-terminal GST fusion proteins by cloning sequences corresponding to amino acids 2–273 of human Stx4 and amino acids 2–262 of Stx3 into pGEX-6P-3 (Amersham Biosciences), which incorporates a PreScission protease (Amersham Biosciences) site in frame between GST and the Stx inserts. GST-StxΔTM proteins were produced in *E. coli* strain BL21(DE3) pLysS after a 4 hr induction with 1 mM IPTG at room temperature. Cells were harvested by centrifugation and lysed by sonication in PBS containing protease inhibitor cocktail (Roche) and 1 mM PMSF. Bacterial lysate containing GST fusion proteins were loaded by gravity onto a column containing 2 ml of packed glutathione sepharose 4B resin. Following binding, the column was washed with 15–20 bed volumes of PBS containing Roche protease inhibitor cocktail and 1 mM PMSF. Recombinant protein was eluted by adding 0.5 ml of PreScission protease (Amersham, 300 units/mL) in 50 mM Tris-HCl, 150 mM NaCl, 1 mM EDTA, 1 mM dithiothreitol (pH 7.0) to the column and incubating overnight at 4°C. Following incubation with protease, the column was washed with 5-10 ml of PBS containing 1 mM DTT to elute the liberated recombinant protein. The protein was purified to > 95% homogeneity as evaluated by Coomassie blue staining. Typically ~5 mg of recombinant protein was purified from a 0.5 L culture. Recombinantly expressed Stx4ΔTM and Stx3ΔTM were soluble up to ~0.4 mg/mL and 0.8 mg/mL, respectively, following cleavage of the N-terminal GST tag. To prepare recording solutions containing Stx peptides, 1 ml of recombinantly expressed StxΔTM protein was dialyzed overnight against 2 × 1L of (in mM): 115 cesium methane sulfonate, 20 $CsCl_2$, 10 HEPES, pH 7.3. Stx3ΔTM and Stx4ΔTM recombinant proteins were diluted into the internal recording solution to a final concentration of 2.5 μM.

Electrophysiology

Transverse hippocampal slices were cut from C57Bl/6 mice (350 μm, ~3 weeks of age, Charles River) in ice cold ACSF (in mM: 87 NaCl, 25 $NaHCO_3$, 2.5 KCl, 1.25 NaH_2PO_4, 0.5 $CaCl_2$, 7 $MgCl_2$, 10 glucose, 1.3 ascorbic acid, saturated with 95% O_2 / 5% CO_2) using a vibratome (Leica VT1000S). Slices were transferred to recording ACSF at 34°C (in mM: 124 NaCl, 3 KCl, 26 $NaHCO_3$, 1.25 NaH_2PO_4, 20 glucose, 2 $CaCl_2$, 1.3 $MgCl_2$) and allowed to return to room temperature for > 45 min. Recordings were made at 28°C in 100 μM picrotoxin to block inhibitory synaptic inputs, and epileptiform bursting was minimized by severing connections between CA3 and CA1 regions and by raising divalent ion concentrations. Whole cell voltage clamp recordings were made from CA1 pyramidal neurons

using IR-DIC optics (pipettes 3-5 MΩ; internal solution, in mM: 130 cesium methylsulfonate, 2.5 NaCl, 5 $MgCl_2$, 0.5 $CaCl_2$, 3 NaATP, 0.5 NaGTP, 0.5 EGTA, 10 phosphocreatine, and 10 HEPES, 0.1 leupeptin). For peptide experiments, internal solutions were supplemented with either Stx4ΔTM or Stx3ΔTM in cesium gluconate to a final concentration of 2.5 μM. Schaffer collaterals were activated at 0.1 Hz using a bipolar stainless steel stimulating electrode (50–200 μA, 100 μsec) and monosynaptic EPSCs were measured at −70 mV with an Axoclamp 700B amplifier and Digidata 1440 digitizer (Molecular Devices). Initial EPSC amplitudes were adjusted to between 75-200 pA. Cells were dialyzed for 9-10 min to allow peptide diffusion, before inducing LTP by pairing depolarization to 0 mV with 200 stimuli at 2 Hz. Recordings and analysis were performed blind to the identity of the peptide. Baseline EPSCs were monitored for > 5 min before pairing and amplitudes were normalized to the baseline period for each experiment. LTP was assessed as EPSC amplitudes 25–30 min after pairing.

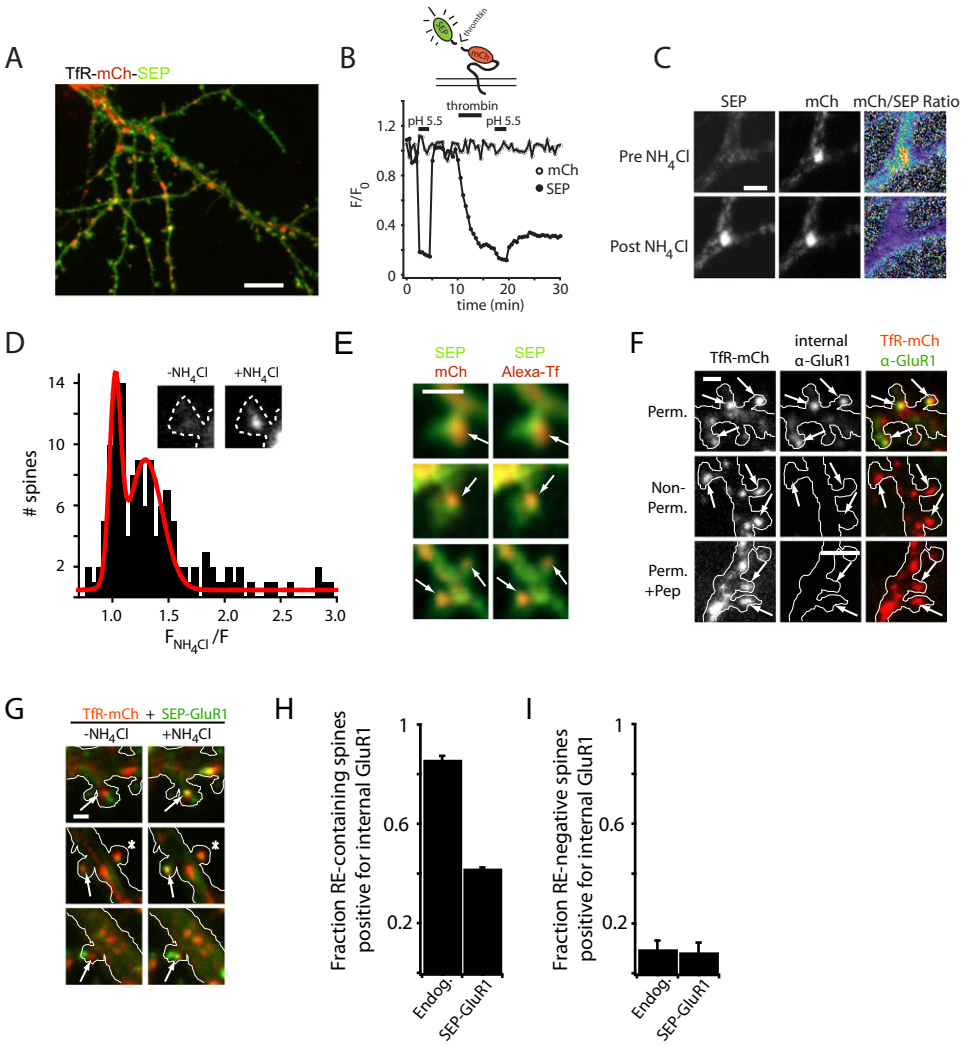

Figure S1. Validation of the TfR-mCh-SEP Reporter, Related to Figure 1

(A) Shown is a hippocampal neuron (DIV18) expressing TfR-mCh-SEP. The large red (mCh) structures are endosomal compartments positive for TfR-mCh-SEP, while the diffuse green (SEP) signal is TfR-mCh-SEP at the plasma membrane. The scale bar represents 10 μm.

(B) The SEP signal originates from TfR-mCh-SEP at the cell surface. Lowering the extracellular pH to 5.5 quenches ~80% of the SEP signal, while the mCh signal is unaffected. A thrombin cleavage site was inserted in the TfR-mCh-SEP reporter between the SEP and mCh sequences (inset).

(C) Determination of the intrinsic mCh/SEP ratio at neutral pH (mCh/SEP_{neut}). Live hippocampal neurons expressing TfR-mCh-SEP were treated with 50 mM NH_4Cl to neutralize intracellular endosomes. Upon neutralization of endosomes, the mCh/SEP ratio becomes homogeneous throughout the neuron.

(D) Quantification of the fraction of RE-positive spines. Live hippocampal neurons expressing TfR-SEP were exposed to extracellular solution containing 50 mM NH_4Cl to neutralize endosomal compartments (inset). The histogram plots the fractional increase in SEP intensity in the presence of NH_4Cl over basal fluorescence for 135 spines from 4 different cells.

(E) TfR-mCh-SEP labels functional recycling compartments in spines. Cells expressing TfR-mCh-SEP were incubated with Alexa647-labeled transferrin (Alexa-Tf) for 30 min. Note the robust Alexa-Tf labeling of spine endosomes (right panels, arrows). The scale bar represents 1 μm.

(F) Controls for anti-GluR1 feeding assay. If cells were not permeabilized (nonperm., middle panels) or if anti-GluR1 was pretreated with the peptide used to raise the antibody (+Pep, bottom panels), no internalized anti-GluR1 was detected. The scale bar represents 1 μm.

(G) Exogenously expressed GluR1 traffics through spine REs. Hippocampal neurons expressing TfR-mCh (red) and SEP-GluR1 (green) were imaged before and after treatment with 50 mM NH_4Cl to visualize endosomal SEP-GluR1. Not all spine REs contained detectable SEP-GluR1 (asterisk). The scale bar represents 1 μm.

(H) Quantification of spine REs positive for endogenous (Endog.) GluR1 or expressed SEP-GluR1 (means ± SEM).

(I) Quantification of endosome-negative spines that label for internalized endogenous (Endog.) GluR1 or expressed SEP-GluR1 (means ± SEM).

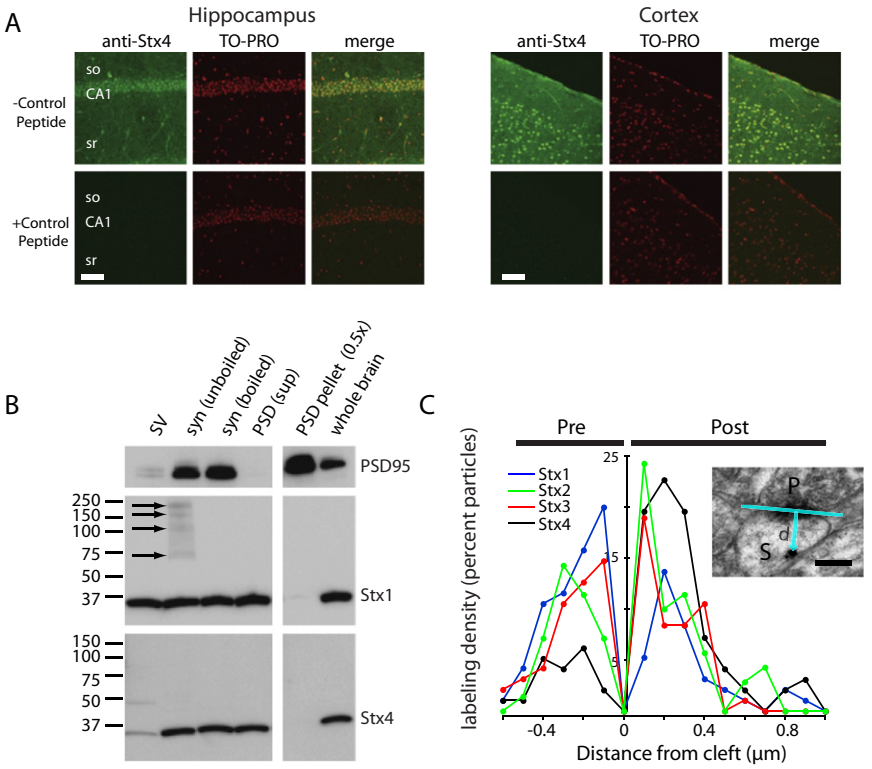

Figure S2. Stx4 is Expressed in Brain and is Postsynaptically Enriched, Related to Figure 4

(A) Immunohistochemical localization of syntaxin-4 (Stx4). Coronal mouse brain sections (50 μm thick) were stained with anti-Stx4 antibody (green) and the nuclear stain TO-PRO (red). Representative labeling from CA1 hippocampus (left) and neocortex (right) are shown. Incubation of the primary antibody with peptide antigen abolished the labeling (+ control peptide). Abbreviations: sr, stratum radiatum; so, stratum oriens. Scale bars, 60 μm.

(B) Immunoblot analysis of mouse brain fractions was performed with antibodies against Stx1 and Stx4. Equal amounts of total protein (12 μg) were loaded for each fraction except for the PSD lane, which was loaded with half as much total protein (6 μg). Note that Stx1 was abundant in the crude synaptic vesicle fraction indicating a large portion of Stx1 is present in presynaptic terminals. Stx4 is present in synaptic fractions but not synaptic vesicles. Unlike Stx1, Stx4 does not form constitutive detergent insoluble high molecular weight complexes (arrows). Neither Stx1 nor Stx4 is strongly associated with the PSD fraction. Abbreviations: SV (crude synaptic vesicles), syn (synaptosome fraction), PSD sup (supernatant from postsynaptic density fraction), PSD (postsynaptic density fraction). Molecular mass markers are shown.

(C) Distribution of syntaxins 1-4 at asymmetric synapses determined by immunogold labeling. The distance (d) of individual gold particles was measured along an axis perpendicular to the synaptic cleft with negative and positive values representing particles at presynaptic and postsynaptic sites, respectively (inset). Stx1 labeling was enriched 2-fold in presynaptic compartments while Stx4 was enriched 4-fold in postsynaptic compartments. Labeling for Stx2 and 3 was distributed more evenly across pre and postsynaptic compartments. Inset scale bar represents 200 nm.

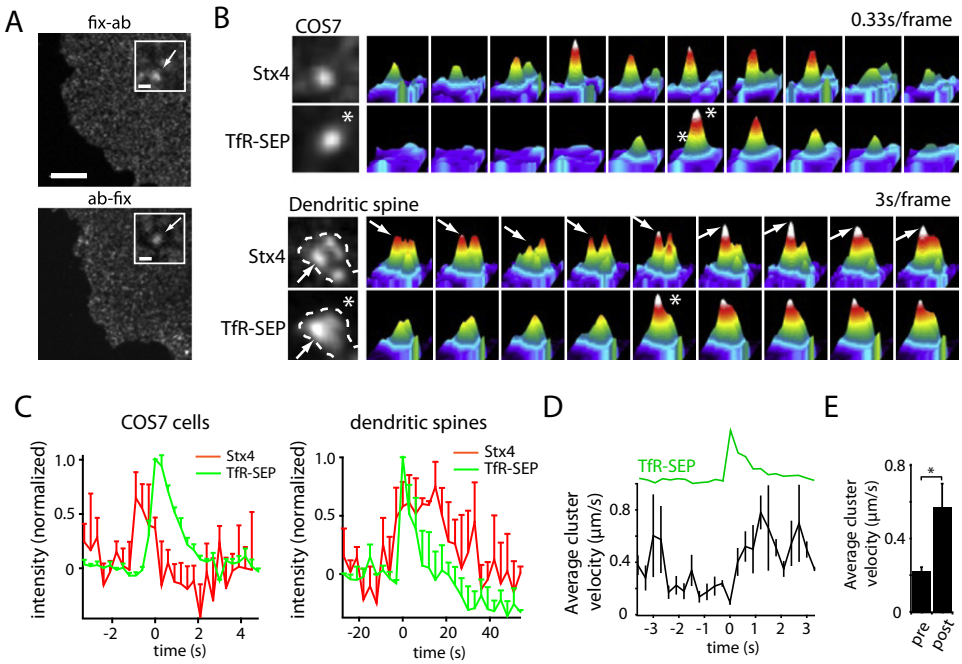

Figure S3. Labeling and Cluster Dynamics of Surface Stx4, Related to Figure 5

(A) Stx4-HA clusters are not caused by antibody-induced cross-linking. COS7 cells expressing Stx4-HA were labeled with anti-HA antibodies and Cy3-conjugated anti-mouse F_{ab} antibody either live (ab-fix), or following fixation (fix-ab). Note the identical clustered appearance of Stx4 in both cases. Arrows indicate individual Stx4 clusters. The scale bar represents 5 μm; inset, 0.5 μm.

(B) Surface-labeled Stx4 cluster intensity was measured during TfR-SEP exocytosis in COS7 cells (top panel) and in dendritic spines (bottom panel). The gray scale image of the first frame when exocytosis was detected (asterisk) is shown to the left.

(C) Surface labeled Stx4 cluster intensity was quantified during TfR-SEP exocytosis in COS7 cells (left panel; n = 6 events) and dendritic spines (right panel) (n = 6 events). Stx4 cluster intensity increased immediately prior to or concomitant with exocytosis. Error bars represent SEM.

(D) Quantification of Stx4 cluster velocity during exocytosis. Note the pausing of the Stx4 cluster immediately prior to exocytosis. Error bars represent SEM, n = 6 events.

(E) Average velocity over a two second time window before exocytosis (pre) and immediately following exocytosis (post).

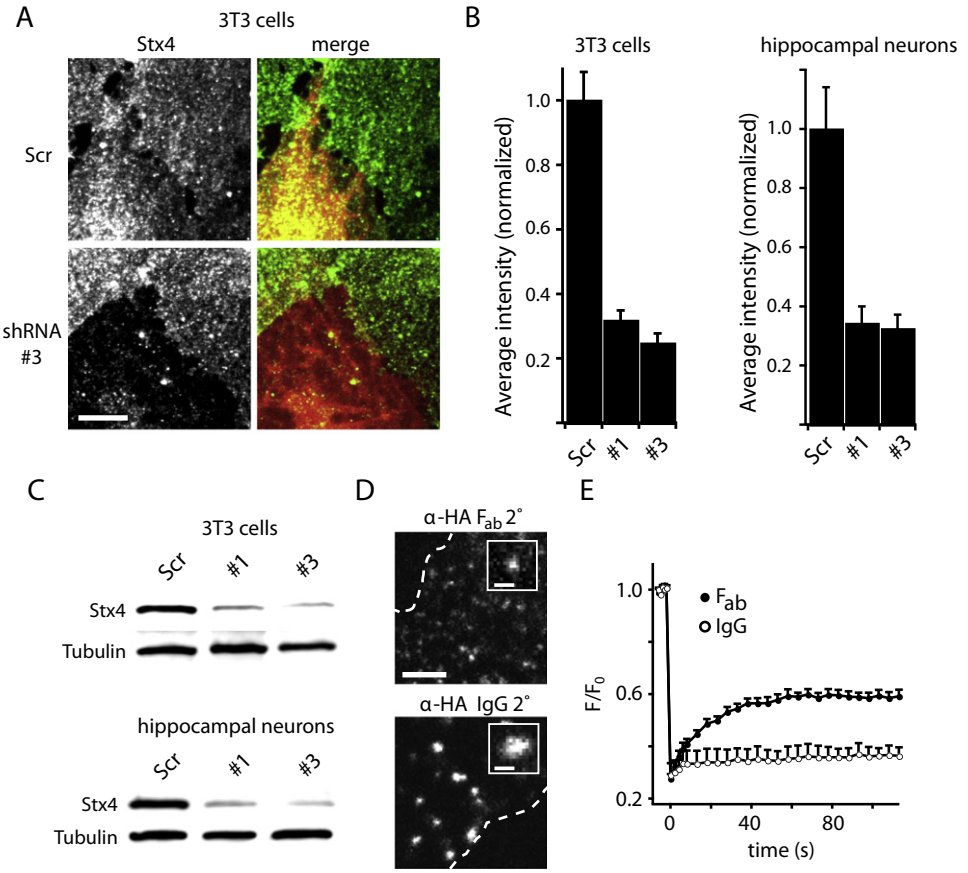

Figure S4. Chronic and Actute Disruption of Stx4 by shRNA and Antibody Crosslinking, Related to Figure 6

(A) 3T3 cells were infected with lentivirus harboring mCherry (red) and Stx4 shRNA #3 or a scrambled control shRNA (Scr) and stained for endogenous Stx4 (green). Note the decrease in endogenous Stx4 labeling in cells expressing Stx4 shRNA (bottom), but not in cells expressing a scrambled control shRNA (top). Scale bar, 5μm.

(B) Quantification of Stx4 staining in 3T3 cells (left) or hippocampal neurons (right) infected with virus expressing scrambled control shRNA (Scr) or two different shRNAs directed against Stx4 (#1, #3).

(C) Immunoblot analysis of Stx4 from 3T3 cultures (top) or hippocampal neurons (bottom) infected with Stx4 shRNAs (#1, #3) or a scrambled control shRNA (Scr) at 5 days postinfection. Tubulin served as a loading control.

(D) Crosslinking of surface Stx4 with IgG secondary. Live COS7 cells expressing Stx4-HA were incubated with mouse monoclonal anti-HA antibody followed by either Cy3-conjugated anti-mouse F_{ab} (upper panel) or Cy3-conjugated anti-mouse whole IgG (lower panel). Large aggregates of surface Stx4 quickly formed upon incubation with bivalent IgG secondary antibody (lower panel) but not monovalent F_{ab} fragments (upper panel). The dashed lines represent cell outlines. Scale bar, 2.5 μm, inset 0.5 μm.

(E) Fluorescence recovery after photobleaching (FRAP) of surface labeled Stx4-HA labeled using Cy3-conjugated F_{ab} or whole IgG anti-HA in COS7 cells. Monovalently labeled Stx4-HA recovered, whereas crosslinking with bivalent IgG severely reduced the mobility of Stx4-HA. Scale bar, 2.5 μm.

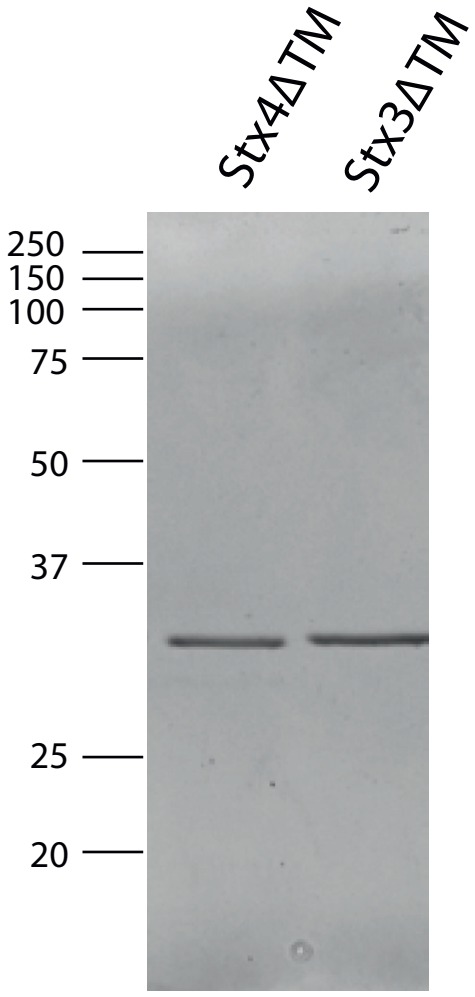

Figure S5. Purity of Recombinant StxΔTM Proteins, Related to Figure 7

Recombinant Stx4ΔTM and Stx3ΔTM were expressed and purified from *E. coli*. Coomassie staining of the purified protein fractions resolved by SDS-PAGE are shown. Molecular mass markers are indicated.